Lithos 190–191 (2014) 204–219

Contents lists available at ScienceDirect

Lithos

journal homepage: www.elsevier.com/locate/lithos

Age constraints on late Mesozoic lithospheric extension and origin of bimodal volcanic rocks from the Hailar basin, NE China

Shuang-Qing Li [a,b,c,*], Ernst Hegner [b,c], Yi-Zeng Yang [a], Jia-De Wu [a], Fukun Chen [a]

[a] Chinese Academy of Sciences, Key Laboratory of Crust–Mantle Materials and Environments, School of Earth and Space Sciences, University of Science and Technology of China, Hefei 230026, China
[b] Department of Earth and Environmental Sciences, LMU Munich, Theresienstr. 41, 80333 Munich, Germany
[c] GeoBio-Center, LMU Munich, Theresienstr. 41, 80333 Munich, Germany

ARTICLE INFO

Article history:
Received 16 September 2013
Accepted 13 December 2013
Available online 24 December 2013

Keywords:
Lithospheric extension
Bimodal volcanism
Magma underplating
Hailar basin
Zircon dating
A-type rhyolite

ABSTRACT

Following the amalgamation of the late Mesoproterozoic–Carboniferous Central Asian Orogenic Belt with the Siberian and North China cratons, NE China underwent late Mesozoic lithospheric extension and widespread formation of volcano-sedimentary basins. We report U–Pb zircon ages and geochemical data for mafic and felsic volcanic rocks from the Hailar basin, located about 1000 km north of Beijing. Zircon populations of six felsic rock samples analyzed by laser ablation ICP-MS yielded similar U–Pb age spectra ranging from 158 to 125 Ma. The youngest zircon ages are interpreted as time of magma eruption and the xenocrystic zircon-age spectra as evidence for a protracted melting of lower crust due to the underplating of mantle-derived magmas during lithospheric extension. The volcanic assemblage has a bimodal composition comprising geochemically evolved trachybasalts and felsic volcanic rocks of I- and subordinate A-type compositions. The mafic volcanic rocks have negative Nb-anomalies, high Th/Nb and Ce/Pb ratios, low initial ε_{Nd} values of +0.4 to +3.4, and radiogenic Pb and Sr isotopes all interpreted as evidence for the melting of passively upwelling asthenosphere and lithospheric mantle previously modified by plate subduction. The xenocrystic zircon ages and chemical/isotopic data of the felsic rocks support an origin from juvenile crustal protoliths: the data of I-type felsic rocks are consistent with the melting of underplated mafic protoliths and those of the A-type rhyolites support the melting of a crustal source with a composition similar to the I-type felsites with apatite controlling their Nb anomaly. The evidence for the persistent melting of a subduction-modified mantle in NE China is in agreement with a model of an extending coupled upper mantle–crust system due to a retreating Paleo-Pacific trench.

© 2013 Elsevier B.V. All rights reserved.

1. Introduction

After the accretion of the late Mesoproterozoic to Carboniferous Central Asian Orogenic Belt (CAOB) with the Siberian and North China cratons (NCC), late Mesozoic extension of the lithosphere in NE China produced a large basin-and-range setting (Graham et al., 2012; Ren et al., 2002) in the CAOB and NCC. Crustal extension was accompanied by exhumation of metamorphic core complexes (Daoudene et al., 2009; Wang et al., 2011), formation of volcano-sedimentary basins (Li et al., 2012; Ren et al., 2002), and emplacement of granitoids and voluminous mafic and felsic volcanic rocks (Wang et al., 2006; Wu et al., 2011; Zhang et al., 2008a). Geochronological data indicate onset of late Mesozoic magmatism in the northern CAOB near the Hailar basin at ca. 160 Ma that lasted until ca. 110 Ma. The age-record of magmatism with volcanic rocks as young as 90 Ma near the Pacific coast have been interpreted as evidence for a SE migration of magmatism (Wang et al., 2006; Zhang et al., 2010). Geochemical data and field observations of the extension-related igneous rocks have documented a predominantly bimodal composition (Ge et al., 2001; Lin et al., 2003) with subduction-related characteristics in the mafic volcanic rocks (Fan et al., 2003; Meng et al., 2011; Xu et al., 2013; Zhang et al., 2008b). Wang et al. (2002) and Zhang et al. (2008b) emphasized the importance of the melting of a subduction-overprinted lithospheric mantle and compared the geological situation in NE China with that of the basin-and-range province of the western United States.

Interpretations of the geodynamic context of late Mesozoic magmatism include a variety of models such as an upwelling mantle plume (Dobretsov and Vernikovsky, 2001; Ge et al., 1999; Lin et al., 2000), post-orogenic collapse of an over-thickened lithosphere after closure of the Mongol–Okhotsk Ocean (Fan et al., 2003; Meng, 2003; Wang et al., 2006), back-arc lithospheric extension due to roll back of the subducting Paleo-Pacific plate (Faure and Natalin, 1992; Li and Shu, 2002; Sun et al., 2013; Zhang et al., 2011; Zhao et al., 1989), and lithospheric delamination (Tomurtogoo et al., 2005; Wang et al., 2006; Wu et al., 2005; Zhang et al., 2010). Recent interpretations of geodynamic models have noted the important role of lithospheric mantle sources that support a passively rifting lithosphere without plume-interaction. Plume involvement appears unlikely as there is no

* Corresponding author at: Chinese Academy of Sciences, Key Laboratory of Crust–Mantle Materials and Environments, School of Earth and Space Sciences, University of Science and Technology of China, Hefei 230026, China. Tel.: +49 89 21804274.
E-mail address: lsq@mail.ustc.edu.cn (S.-Q. Li).

0024-4937/$ – see front matter © 2013 Elsevier B.V. All rights reserved.
http://dx.doi.org/10.1016/j.lithos.2013.12.009

evidence for active rifting and lithospheric updoming, plume-related high-degree magmas such as picrites, olivine tholeiites, and tholeiitic basaltic magmas, as well as plume-related Fe–Ti–V and Ni–Cr–Platinum Group Element (PGE) deposits such as, for example, related to the ca. 260 Ma old Emeishan flood basalt province in China (e.g., He et al., 2007; Luo et al., 2013, 2014; Wang et al., 1989; Zhang et al., 2006; Zhou et al., 2013). In addition, the typically very short time-scales of massive volcanic eruptions over mantle plumes is contrasted by a protracted period of magmatism of 60 to 80 Ma in NE China.

In this study of mafic and felsic volcanic rocks from the region of the late Mesozoic Hailar basin in NE China, we constrain the duration of lower crustal reworking during lithospheric extension and interpret the geochemical data as evidence for the composition and temporal variation of magma sources with ongoing lithospheric thinning.

2. Geology of study area and description of samples

The late Mesozoic Hailar basin is located about 1000 km north of Beijing in the northern part of the late Mesoproterozoic to Carboniferous CAOB (e.g., Dobretsov et al., 1995; Sengör et al., 1993; Windley et al., 2007; Xiao et al., 2003). It is situated to the south of the Mongol–Okhotsk suture that closed around 160–140 Ma in this part of the CAOB (e.g., Zorin, 1999) and on the western flank of the Great Xing'an range, an uplifted section in the extending CAOB (Fig. 1a). The basin has a NE-trending axis and comprises an assemblage of predominantly mafic volcanic rocks at the bottom (Tamulangou Formation; abbreviated below as Fm.) and felsic volcanic rocks at the top (Shangkuli Fm.). The igneous rock section is overlain by non-marine sedimentary rocks ranging in age from ca. 140 Ma to Recent (A et al., 2013; IMBGMR, 1991; Zhang and Long, 1995). A drill core profile from the Hailar basin shows a highly weathered CAOB basement overlain by a 1 km thick volcanic sequence with mainly mafic volcanic rocks at the base and felsic volcanic rocks and minor intercalated basalts and sedimentary rocks at the top. The overlying 3 km thick sediment package consists of mud- and siltstones deposited from ca. 100 Ma to Recent (Gao et al., 2009; Wan, 2006).

In the study area, late Mesozoic volcanic rocks were deposited over large areas in an evolving basin-and-range setting (Graham et al., 2012). Geochronological studies of late Mesozoic volcanic rocks from the Hailar region (Chen et al., 2006; Gou et al., 2013; Meng et al., 2011; Wang et al., 2006; Wu et al., 2011; Zhang et al., 2008a) indicate contemporaneous eruption of mafic and felsic rocks (albeit more mafic rocks at the beginning of volcanism), and intrusion of granitoids from ca. 160 to 110 Ma. Geochemical and Sr and Nd isotopic data for mafic and felsic volcanic rocks have been interpreted as evidence for calc-alkaline compositions and the melting of subduction-modified mantle sources with low ε_{Nd} values of −1 to +4 (Fan et al., 2003; Guo et al., 2010; Zhang et al., 2008b).

The basement in the region of the Hailar basin comprises late Paleozoic ca. 360 to 295 Ma metavolcano-sedimentary assemblages of the CAOB (Budate Group; Wan, 2006) and intrusive granitoids of ca. 282 to 295 Ma (Meng et al., 2013). Initial ε_{Nd} values of −2 to +6 for similar CAOB assemblages to the SW of the Hailar basin (Chen et al., 2009) were interpreted as overall juvenile continental magmatic arcs with a significant proportion of late Neoproterozoic material (Zhao et al., 2010). This type of basement had evolved isotopically to ε_{Nd} values of 0 to −6 at the time of late Mesozoic volcanism in the Hailar basin.

Thirteen basaltic-trachyandesite samples were collected from areas mapped as the lower Tamulangou Fm. at the western and northern margins of the Hailar basin (Fig. 1b, Table 1). The map shows outcrops of mafic volcanic rocks mapped as the lower Tamulangou Fm. We have not determined ages on these samples and it is therefore not clear if they indeed belong to the lower Tamulangou Fm., or represent some of the subordinate mafic lavas intercalated with the felsic rocks of the upper Shangkuli Fm. For other areas also mapped as Tamulangou Fm., U–Pb zircon ages (Chen et al., 2006; Ying et al., 2010) and Ar–Ar whole-rock ages (Wang et al., 2006; Zhang et al., 2008a) yielded an age spectrum ranging from ca. 180 to 140 Ma. U–Pb zircon ages for subordinate felsic lavas associated with the mafic volcanic rocks may be taken as firm evidence for the deposition of the lower mafic volcanic rocks from ca. 160 Ma to 140 Ma (Ying et al., 2010; Zhang et al., 2008a). The mafic rock samples are mostly subaphyric to weakly porphyritic and show phenocrysts of pyroxene and plagioclase, and subordinate amounts of amphibole. The matrix is aphanitic or composed of fine-grained clinopyroxene, plagioclase, biotite, and a few opaque oxide minerals. Common are vesicles filled with agate or calcite.

The felsic volcanic rocks of the upper Shangkuli Fm. are widespread in the Hailar area and were sampled at the western and northern margins of the basin (Fig. 1b). U–Pb dating of zircons yielded crystallization ages of 140 to 110 Ma (Ying et al., 2010; Zhang et al., 2008a). The Shangkuli Fm. comprises trachytes and rhyodacites, interlayered with pyroclastic tuffs, volcanic sandstone, rhyodacitic lavas, and subordinate basaltic lava flows. The rhyolites and dacites have a porphyritic texture, with phenocrysts set in a glassy matrix. Flow banding, spherulitic and perlitic structures are common. The phenocrysts are sanidine, quartz, plagioclase, and biotite. The matrix of the trachytes shows fine-grained plagioclase and hornblende and a few opaque oxide minerals. The rhyolitic tuffs contain broken phenocrysts of quartz and feldspar set in a devitrified, microcrystalline groundmass. From this unit we analyzed seventeen felsic rock samples and dated zircons of one trachyte and five rhyolite samples by laser ablation ICP-MS.

3. Analytical methods

The zircon concentrates were prepared by hand-panning of the <500 μm grain-size fraction of the samples and magnetic- and heavy-liquid mineral separation techniques (Hou et al., 2010). Three basaltic trachyandesites that were also processed provided no zircons and we consider this finding as good evidence for the absence of magma contamination by felsic material in these mafic volcanic rocks. More than 100 zircon crystals of each sample were handpicked under a binocular microscope for analysis. The samples show similar populations of apparently magmatic zircons, only differing in size. The grains selected for analysis were transparent, colorless, and mostly subangular with some crystals showing well-defined prisms and euhedral to subhedral habitus. Under the binocular and also in cathode luminescence (CL) images there is no evidence for zircon cores, and typical xenocrystic or detrital grains, although as shown in Section 4.1 most of them are inherited xenocrysts. The zircons were placed on adhesive tape, embedded in epoxy resin, and polished to about half of their thickness. CL images of the internal structures were taken with a Cameca SX-50 microprobe at the Institute of Geology and Geophysics, Chinese Academy of Sciences (CAS), Beijing. The zircon grains show a diffuse oscillatory magmatic zoning and the analyzed grains yielded typical magmatic Th/U ratios >0.5 (Table S1; Hoskin and Schaltegger, 2003). U–Pb isotopic analyses were carried out at the Key Laboratory of Crust–Mantle Materials and Environments of CAS at the University of Science and Technology of China (USTC), Hefei. We used an inductively-coupled plasma mass spectrometer (LA–ICP-MS; Perkin Elmer Elan DRC II) equipped with a Microlas system (GeoLas 200 M, 193 nm ArF-excimer laser). The diameter of the laser-ablation pits was approximately 40 μm and the average power output about 4 W. Signal and background measuring times were 70 and 40 s, respectively. U, Th, and Pb concentrations were calibrated against the NIST610 reference material which was measured twice every 10 sample spots. The age calculations were calibrated against Zircon 91500 reference material analyzed after every fifth sample spot. In order to avoid an age bias due to selective analysis of a certain type of zircon and specific zircon domains, cores and rims of more than fifty grains of different sizes were randomly analyzed. More details on the laser-ablation U–Pb dating technique are given in Liu et al. (2007). The conventional correction procedure

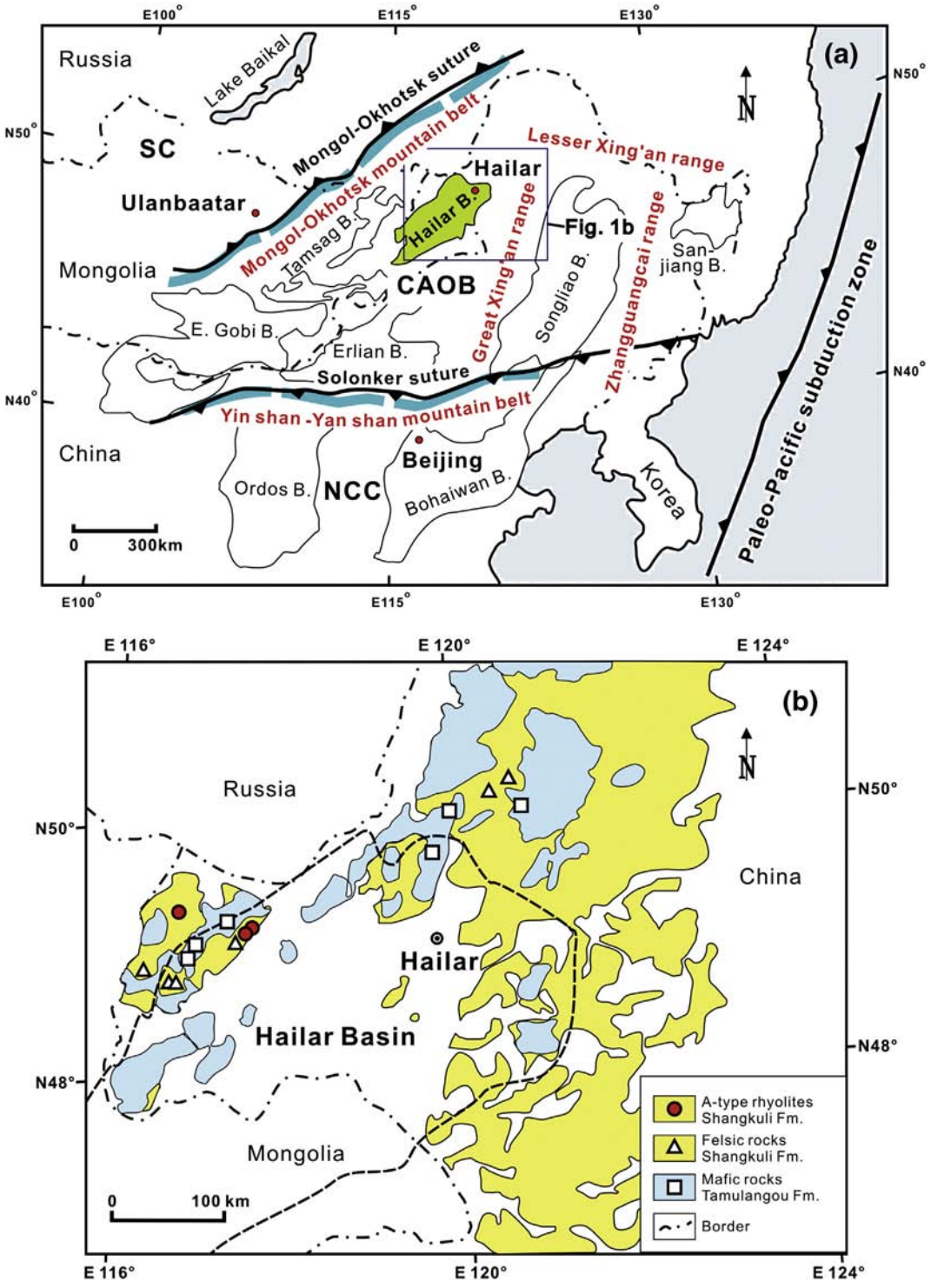

Fig. 1. Geological sketch maps showing NE China and the study area at the Hailar basin. (a) Map showing the location of the study area in the Central Asian Orogenic Belt (CAOB) and bordering Mongol–Okhotsk and Solonker sutures. The major late Mesozoic volcano-sedimentary basins in the CAOB and bordering cratons are outlined. Abbreviations: SC—Siberian Craton, CAOB—Central Asian Orogenic Belt, NCC—North China Craton, Fm.—Formation. Map simplified from Meng (2003) and Wang et al. (2011); sutures and subduction polarities from Ritts et al. (2001) and Wang et al. (2011). (b) Map of the Hailar region showing the basin margin and distribution of mafic and felsic volcanic rocks (modified after Wang et al., 2006; Zhang et al., 2008b). The sample localities are indicated.

for common lead could not be used due to the low ^{204}Pb signal and interfering ^{204}Hg from Ar. We used instead the procedure "ComPbCorr#3_18" of Andersen (2002) which solves for the mass-balance caused by the combined effects of common lead and lead loss at a specific time. The U–Pb raw data were processed with Glitter 4.0 (Macquarie University, Australia) and the U–Pb ages were calculated with ISOPLOT 3 (Ludwig, 2003). During the course of this study fifty-seven spots analyzed on Zircon 91500 yielded a mean ^{207}Pb/^{206}Pb age of 1062 ± 16 Ma (2SD) and a mean ^{238}U/^{206}Pb age of 1062 ± 8 Ma (2SD). Errors of the U–Pb zircon ages in this paper refer to the 2σ confidence level, except for those listed in Table S1. We report here the ages of the ^{238}U–^{206}Pb decay system because of its high precision for young rocks.

The whole-rock samples were crushed and chips free of weathered material and amygdules were ground in a tungsten-carbide mill.

Table 1
Sample localities and eruption ages of late Mesozoic volcanic rocks from the Hailar basin, NE China.

Basaltic trachyandesite—mapped as lower Tamulangou Fm.			
FK10-98	48°51′18.11″ N; 116°58′58.72″ E	Basaltic trachyandesite	
FK10-99	48°51′18.62″ N; 116°58′59.52″ E	Basaltic trachyandesite	
FK10-96	48°51′15.57″ N; 116°58′57.08″ E	Basaltic trachyandesite	
FK10-97	48°51′15.57″ N; 116°58′57.08″ E	Trachyandesite	
FK10-100	48°51′33.90″ N; 116°59′14.49″ E	Basaltic trachyandesite	
FK10-101	48°52′49.02″ N; 117°00′29.97″ E	Basaltic trachyandesite	
FK10-78	49°13′26.22″ N; 117°28′28.48″ E	Basaltic trachyandesite	
FK10-79	49°13′30.91″ N; 117°28′33.02″ E	Basaltic trachyandesite	
FK10-77	49°13′26.22″ N; 117°28′28.48″ E	Basaltic trachyandesite	
FK10-116*	49°50′33.79″ N; 119°57′33.99″ E	Basaltic trachyandesite	
FK10-111*	50°12′31.88″ N; 119°38′48.83″ E	Trachyandesite	
FK10-112*	50°07′52.00″ N; 120°12′26.41″ E	Basaltic trachyandesite	
FK10-113*	50°07′52.00″ N; 120°12′26.41″ E	Basaltic trachyandesite	
Trachyte and I-type rhyodacite—ca. 140 to 120 Ma upper Shangkuli Fm.			
FK10-80	49°17′23.51″ N; 117°32′4.53″ E	Trachyte	132 ± 6 Ma[a]
FK10-81	49°17′23.51″ N; 117°32′4.53″ E	Trachyte	
FK10-102	48°46′32.07″ N; 116°17′05.1″ E	Dacite	
FK10-104	48°37′19.26″ N; 116°49′9.91″ E	Dacite	
FK10-105	48°37′18.97″ N; 116°49′8.90″ E	Rhyolite	
FK10-107*	50°14′43.88″ N; 120°28′4.09″ E	Dacite	
FK10-108*	50°14′43.88″ N; 120°28′4.09″ E	Rhyolite	
05GH11	50°26′22.06″ N; 120°48′12.6″ E	Rhyolite	124 ± 5 Ma[b]
A-type rhyolite—upper Shangkuli Fm.			
FK10-83	49°17′35.35″ N; 117°32′29.66″ E	A-type rhyolite	136 ± 8 Ma[a]
FK10-87	49°18′34.99″ N; 117°33′12.86″ E	A-type rhyolite	134 ± 4 Ma[a]
FK10-86	49°18′25.00″ N; 117°33′01.00″ E	A-type rhyolite	
FK10-88	49°18′47.20″ N; 117°33′37.42″ E	A-type rhyolite	133 ± 4 Ma[a]
FK10-89	49°18′57.48″ N; 117°34′04.91″ E	A-type rhyolite	
FK10-90	49°23′47.95″ N; 117°07′51.56″ E	A-type rhyolite	
FK10-91	49°23′47.95″ N; 117°07′51.56″ E	A-type rhyolite	
FK10-82	49°17′24.05″ N; 117°32′06.05″ E	Rhyolitic tuff	126 ± 6 Ma[a]
FK10-84	49°18′04.28″ N; 117°32′45.81″ E	Rhyolitic tuff	125 ± 6 Ma[a]
FK10-85	49°18′04.28″ N; 117°32′45.81″ E	Rhyolitic tuff	

* Sample locality north of Hailar, other samples from west of Hailar.
[a] This study, youngest single spot U–Pb zircon ages interpreted as the eruption age.
[b] U–Pb zircon age (LA–ICP-MS), Ying et al. (2010). Errors are 2σ.

Major-element concentrations were determined on glass tablets at CAS Beijing with wavelength-dispersive X-ray fluorescence spectrometry (SHIMADZU XRF 1500 spectrometer; method described in Guo et al., 2006). Loss-on-ignition (LOI) was determined on about 5 g of sample powders baked at 1000 °C for 1 h. The precision of the major-element concentrations are ≤3%, and the accuracy as determined on the Chinese whole-rock standards GSR-1 and GSR-3 (Xie et al., 1985) are around 5% (2σ) (Table S2).

For trace-element analysis the sample powders were digested in a mixture of HF and HNO_3 in high-pressure Teflon bombs for two days. The sample solutions were analyzed with the Elan DRC-II-ICP-MS at USTC using the procedures described in Hou and Wang (2007). Ruthenium was used as an internal standard to correct for matrix effects and instrument drift. The total procedure blank of <35 ng for all elements is not significant for the analyzed element concentrations. The precision of the trace element data is about 5% and the accuracy of the data ≤5% for most elements as has been estimated from analyses of the USGS rock standards BHVO-2 and AGV-2 (Table S2).

The Sm–Nd, Rb–Sr, and Pb isotopic analyses were carried out at USTC and nine Sr isotopic analyses at LMU Munich according to the methods of Chen et al. (2000) and Hegner et al. (1995), respectively. Sm, Nd, Rb, and Sr concentrations were determined by isotopic dilution using ^{149}Sm, ^{150}Nd, ^{84}Sr, and ^{85}Rb tracers. The isotopic abundance ratios were determined on a Finnigan MAT 262 (USTC) and an upgraded MAT 261 mass spectrometer (LMU). $^{143}Nd/^{144}Nd$ ratios are normalized to $^{146}Nd/^{144}Nd = 0.7219$, Sm isotopic ratios to $^{147}Sm/^{152}Sm = 0.56081$, and $^{87}Sr/^{86}Sr$ ratios to $^{86}Sr/^{88}Sr = 0.1194$ using a Rayleigh fractionation law. During the course of this study, analyses of the La Jolla reference solution yielded $^{143}Nd/^{144}Nd = 0.511869 \pm 0.000006$ (2SD, n = 25) and NIST 987 yielded $^{87}Sr/^{86}Sr$ ratios of 0.710249 ± 0.000012 (2SD, n = 38; USTC) and 0.710243 ± 0.000004 (2SD, n = 9; LMU, indistinguishable within-error from the USTC data). Measured Pb isotopic ratios were corrected for thermal mass fractionation using a value of 0.11% per atomic mass unit as has been inferred from analysis of the reference material NIST 981.

4. Results and discussion

4.1. Zircon-age record in felsic rocks

The laser-ablation ICP-MS zircon-spot ages for six felsic volcanic rock samples from the upper Shangkuli Fm. are shown in concordia diagrams and histograms in Fig. 2. The U–Pb isotope ratios and corresponding ages are listed in Table S1. The samples were collected at the western margin of the Hailar basin (Fig. 1b) from an approximately 2 km long section of NE dipping lavas of trachytic to rhyolitic composition, altogether up to almost 500 m thick. Two tuff and one rhyolite samples were collected in an about 12 m wide outcrop near the base of the volcanic sequence. Sample FK10-82 was collected from a tuff bed directly underlying a rhyolite lava (sample FK10-83) which is overlain by another tuff bed (sample FK10-84). Fifty-seven spot analyses on zircon grains from the lower tuff sample FK10-82 gave within-error concordant data points with $^{206}Pb/^{238}U$ ages ranging from 147 ± 4 Ma (2SD) to 126 ± 6 Ma (2SD, Fig. 2b). Although there is significant overlap of the error ellipsoids of adjacent data points, distinct mean ages are indicated by the statistically significant differences at the 95% confidence interval between the youngest and oldest zircons grains. Thirty-eight zircon spots for the upper tuff sample FK10-84 show a similar concordant age spectrum with $^{206}Pb/^{238}U$ ages ranging from 154 ± 10 Ma to 125 ± 6 Ma (Fig. 2d). The youngest spot ages in both tuff samples agree within error limits and we suggest an eruption age for the tuffs of ca. 125 Ma. The zircon grains with ages up to 154 Ma are apparently xenocrysts inherited from felsic crustal protoliths of the tuff samples that crystallized during crustal extension and formation of the Hailar basin (see Section 4.5).

The $^{206}Pb/^{238}U$ ages of forty-seven zircon spots for the interlayered rhyolite sample FK10-83 are concordant within-error and range from 158 ± 6 Ma to 136 ± 4 Ma. By inference, 136 Ma is interpreted as maximum eruption age and it can be seen that this date is much older than the ca. 125 Ma ages that we obtained of the bracketing tuff samples. Thus, taking the geological constraints into account, rhyolite sample FK10-83 must also be ca. 125 Ma old. Apparently, the zircon grains selected for analysis of rhyolite sample FK10-83 included only older xenocrystic varieties and hand-picking missed those that crystallized from the erupted magma.

Rhyolite samples FK10-87 and FK10-88 were collected from two adjacent 3–4 m thick flows from the top of the cross-section, stratigraphically approximately 500 m above the dated tuffs and therefore should be younger than 125 Ma as determined for the base section of the volcanic package. Forty-two concordant $^{206}Pb/^{238}U$ zircon-spot ages for sample FK10-87 range from 149 ± 2 Ma to 134 ± 4 Ma, and fifty-four zircon spots for sample FK10-88 gave within-error concordant $^{206}Pb/^{238}U$ ages ranging from 148 ± 4 Ma to 133 ± 4 Ma (Fig. 2e, f). The youngest zircon age for these samples suggests eruption at ca. 134 Ma which is excessively old considering their stratigraphic position above the tuff samples. Therefore we accept the 125 Ma age of the tuff samples as maximum age for the emplacement of these rhyolites. The zircon-age spectra in these samples agree with those of the other samples from

the cross section and indicate the melting of felsic crustal sources with crystallization ages ranging from ca. 158 to 133 Ma. This age-span coincides with the beginning and much of the intermediate period of lithospheric extension and basin development as has been determined from age dating of surface samples (Xu et al., 2013; Zhang et al., 2008a).

Trachyte sample FK10-81 was collected from a lava flow about 10 m below the dated basal tuff-rhyolite section. A total of sixty-six zircon spots yielded within-error concordant data points with $^{206}Pb/^{238}U$ ages ranging from 149 ± 6 Ma to 132 ± 6 Ma (Fig. 2a). The youngest zircon age of 132 Ma is consistent with the stratigraphic position of the sample below the dated tuffs-rhyolite section.

The zircon-age spectra in the felsic rocks provide an interesting view on ongoing crustal melting, magma crystallization, and compositional modification of the source rocks during lithospheric extension and it needs to be assessed if Pb-loss and resetting of the U–Pb clock could be responsible for the variation in zircon ages. Pb-loss in young zircons cannot be easily identified in the Wetherill diagram (Wetherill, 1956) from the degree of concordancy of the data point because Pb-loss would move the data point along the concordia due to its steep slope near the origin. We plotted the data in a Tera–Wasserburg diagram with a stronger curvature of the concordia near the origin which makes it easier to detect Pb-loss and discordant data points, but found no evidence for Pb-loss. There are a number of observations suggesting that the zircon-age spectrum was not biased by Pb-loss: for example, the zircon-spot ages for cores and rims are indistinguishable which would not be the case if the grains had undergone Pb-loss that affects rims more readily than cores. In addition, the analysis of small zircon grains that undergo a higher degree of Pb-loss than big grains did not

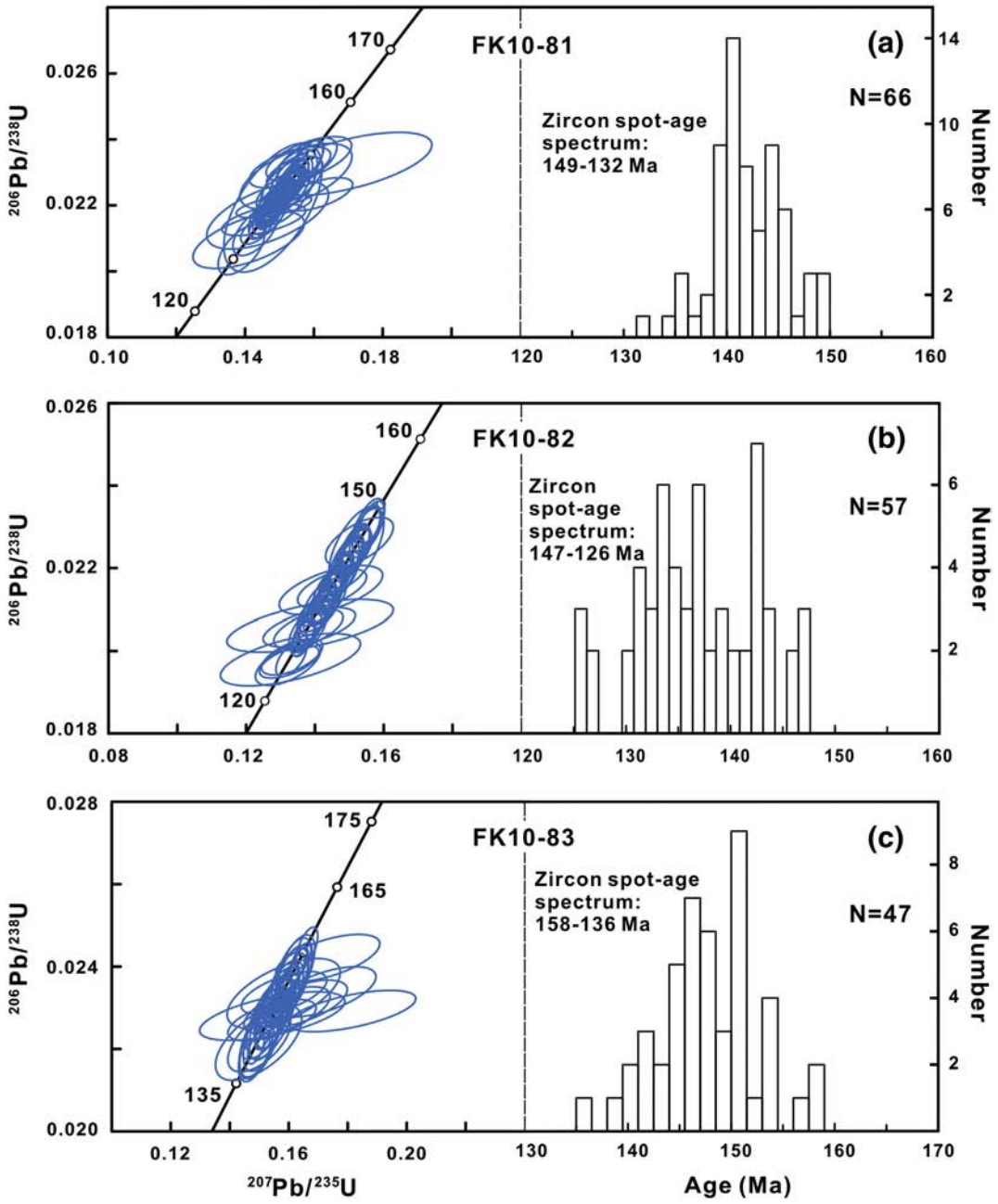

Fig. 2. Concordia diagrams for laser ablation ICP-MS zircon analyses of late Mesozoic A-type rhyolite and trachyte samples from the Hailar basin, NE China. The error envelopes indicate 1σ age uncertainties. The histograms show the age distribution of the zircon-spot analyses (N = number of spots). The lowest zircon age of each sample is interpreted as the maximum age of magma eruption; older ages are interpreted to reflect those of xenocrystic zircons inherited from the source of the felsite samples.

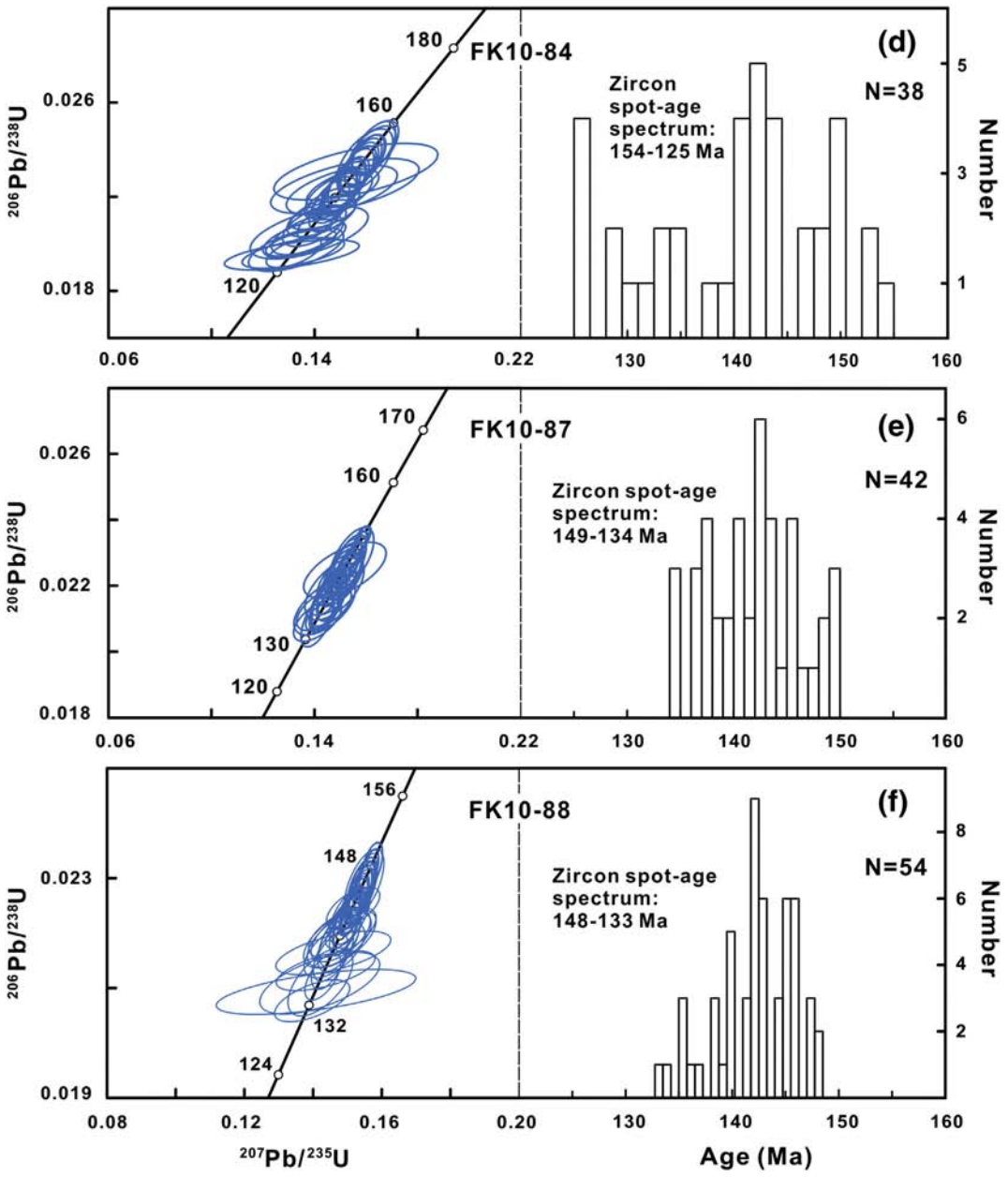

Fig. 2 (*continued*).

produce younger ages. Moreover, the broad agreement of a Rb–Sr whole-rock age of 131 ± 5 Ma (MSWD = 20; 12 samples from Ge et al., 2001, and this study) with the emplacement age of ca. 125 Ma inferred from the zircons in the same samples also suggests that Pb loss is probably not the reason of the age variation. Due to the fact that the dated felsic samples belong to the ca. 140 to 110 Ma old Shangkuli Fm. (Meng et al., 2011; Zhang et al., 2008a), zircon ages up to 158 Ma must reflect xenocrystic grains. Finally, the zircon-age spectrum of zircons in our samples overlaps the ages determined on other felsic rocks from the Hailar region (Chen et al., 2006; Meng et al., 2011; Zhang et al., 2008a). Thus, we interpret the youngest zircon ages as constraints on magma eruption and the older ages as xenocrystic zircon ages reflecting magma crystallization in the source of the felsites.

In summary, the six felsic rock samples dated in this study show similar zircon-age spectra of ca. 158 to 125 Ma. The age spectra agree with the inferred onset and much of the duration of basin-related magmatism in the Hailar region (Meng et al., 2011; Ying et al., 2010; Zhang et al., 2008a) and show that lithospheric extension and volcanism was accompanied by major crustal melting and crystallization of felsic material at lower crustal levels. The predominance of ca. 140–130 Ma xenocrystic zircons in the samples in combination with the large volume of felsic rocks suggests that at this stage of lithospheric extension, temperatures in the lower crust must have been sufficiently high for large-scale melting and that this felsic material is a major source of the analyzed samples. There is no evidence for older zircons from the CAOB basement in our samples which shows that reworking of juvenile material rather than the CAOB basement was important for the rhyolites of this study.

As will be discussed in detail in Section 4.3, some of the dated felsic rock samples are A-type rhyolites and they represent a rare rock type in the Hailar basin. Our zircon ages show that A-type rhyolites were erupted at ca. 125 Ma; I-type felsites, for which a single trachyte sample dated in this study gave an age of 132 Ma, were produced in small

volumes during the beginning of magmatism and represent the predominant rock type during the mature stage of lithospheric extension.

4.2. Geochemical constraints on the source of mantle-derived volcanic rocks

Representative major- and trace-element data for the late Mesozoic volcanic rocks from the Hailar basin are shown in Table 2 and the data for all samples are reported in the on-line Table S3. The Sr–Nd isotopic data and Pb isotopic data of whole-rock samples are in Table 3 and the on-line Table S4. The major element concentrations (Fig. 3) suggest a bimodal assemblage consistent with evidence from drill cores and field observations for predominantly mafic rocks at the base of the volcanic pile (Tamulangou Fm.) and an increasing abundance of felsic volcanic rocks and fewer interlayered mafic lavas in the Shangkuli Fm. at the top of the volcanic sequence (IMBGMR, 1991). The thirteen samples of mafic composition of this study comprise basaltic trachyandesites, trachyandesites, and trachytes (Fig. 3) representing typical compositions of intra-plate settings (Bailey, 1974). Contrary to some previous reports (e.g., Fan et al., 2003; Zhang et al., 2008b), we note that our samples have alkaline compositions and are thus different from calc-alkaline rock types belonging to the subalkaline family of rocks.

Low Mg-numbers of 52 to 23 and low Ni, Cr and Sc concentrations in the mafic samples indicate moderate to extensive crystal fractionation of olivine and clinopyroxene, respectively (Tables 2, S3). The magmas also have undergone shallow-level plagioclase fractionation as indicated by their small Eu-anomalies (Fig. 4a). The REE patterns of the samples are very similar with moderate to strong LREE/HREE fractionation ($(La/Yb)_N$ of 10 to 40) and Gd/Yb ratios of 3 to 6 implying variable amounts of residual garnet in the mantle sources during partial melting.

There is abundant geochemical evidence for the melting of subduction-modified mantle sources including an old sediment component: the extended REE patterns (Fig. 4a) show a distinct

Table 2
Representative major- and trace-element concentrations for late Mesozoic volcanic rocks from the Hailar basin, NE China (see on-line supplement S2 for more data).

	Basaltic trachyandesite			Trachyte and I-type rhyodacite			A-type rhyolite		
	FK10-98	FK10-78	FK10-111	FK10-80	FK10-104	FK10-108	FK10-83	FK10-90	FK10-84
SiO_2	51.89	53.96	57.68	63.96	67.56	70.29	77.31	75.36	77.01
TiO_2	2.39	1.9	1.48	0.7	0.48	0.22	0.2	0.24	0.2
Al_2O_3	17.16	15.77	18.46	16.77	14.68	14.62	12.39	12.66	12.01
Fe_2O_3t[a]	9.98	8.99	6.76	2.86	2.86	1.7	0.82	1.52	0.74
MnO	0.13	0.1	0.07	0.07	0.15	0.07	0.01	0.03	0.01
MgO	2.55	3.34	1.03	0.94	1.21	0.28	0.12	0.28	0.15
CaO	5.95	6.08	4.32	2.14	1.53	0.7	0.08	0.2	0.22
Na_2O	4.05	3.98	4.78	4.53	2.67	4.51	4.26	3.78	3.94
K_2O	2.42	2.76	3.08	4.77	3.3	4.63	4.77	4.99	5.2
P_2O_5	1.19	1.07	0.79	0.17	0.08	0.06	0.03	0.03	0.03
LOI	1.96	1.42	1.82	3.58	5.84	3.36	0.44	1.2	0.7
Total	99.67	99.37	100.27	100.49	100.36	100.44	100.43	100.29	100.21
Mg#[b]	34	43	23						
Sc	36	32	18	13	3.7	1.6	4.1	4.7	4
Cr	21	90	78	21	20	3	24	20	14
Co	7	13	14	1.7	3.8	0.83	3.4	2.8	0.65
Ni	22	38	37	5.8	11	2.9	8	6.9	2
Ga	26	24	26	21	20	12	24	24	24
Rb[c]	67.7	60.1	59.9	159	149	105	224	219	243
Sr[c]	757	799	960	345	227	71	16.7	15.5	17
Y	24	22	13	24	24	13	46	38	44
Zr	391	370	479	509	195	180	305	375	304
Nb	17	20	13	20	15	10	47	45	47
Cs	0.45	0.71	2.2	7.1	8.8	10	3.3	3.7	7.4
Ba	922	865	1124	1314	281	342	41	19	25
La	54	65	55	61	46	45	39	47	41
Ce	134	149	108	117	98	90	94	88	96
Pr	15	16	13	14	11	9.1	11	12	11
Nd[c]	66.14	64.87	48.15	56.82	37.61	28.85	40.38	46.2	37.9
Sm[c]	12.08	11.4	8.142	9.795	7.339	4.901	9.734	10.04	8.844
Eu	2.8	2.7	2.2	2.3	1.1	0.65	0.29	0.36	0.25
Gd	8.8	8.6	6	7	6.5	4.2	8.1	7.7	7.6
Tb	1.1	0.97	0.67	0.86	0.89	0.57	1.2	1.1	1.2
Dy	5.2	4.6	3.1	4.4	4.9	3	7	6.2	6.8
Ho	0.92	0.77	0.48	0.8	0.88	0.53	1.4	1.2	1.4
Er	2.3	1.9	1.2	2.1	2.4	1.4	3.8	3.3	3.7
Tm	0.3	0.24	0.15	0.29	0.36	0.21	0.58	0.49	0.57
Yb	1.9	1.5	0.93	2	2.4	1.4	3.9	3.4	4
Lu	0.27	0.22	0.13	0.31	0.35	0.21	0.58	0.5	0.59
Hf	8.9	8.2	6.9	11	5.7	5.1	10	12	10
Ta	0.6	0.83	0.69	1.1	1.2	1.1	2.7	2.5	2.6
Pb	16	15	18	22	26	21	32	18	15
Th	6.1	5.7	6.9	14	18	21	34	31	36
U	1.6	1.6	1.2	4.1	8.7	4.5	12	4.1	15
Nb/La	0.31	0.31	0.24	0.33	0.33	0.23	1.2	0.96	1.2
Eu/Eu*[d]	0.85	0.83	0.94	0.91	0.47	0.42	0.1	0.13	0.09
Ce/Pb	8.4	9.9	6	5.3	3.8	4.3	2.9	4.9	6.4
$(La/Yb)_N$	20	30	42	22	14	23	7.1	9.8	7.4

Major element concentrations in wt.%, trace element data as ppm. LOI = loss on ignition.
[a] Total Fe as Fe_2O_3.
[b] Mg# = 100 × molar $Mg^{2+}/(Mg^{2+}+Fe^{2+t})$.
[c] Determined by isotope dilution.
[d] $Eu/Eu^* = Eu_N/(Sm_N \times Gd_N)^{0.5}$; N = concentration normalized to chondrite value (Boynton, 1984).

Table 3
$^{87}Sr/^{86}Sr$ and $^{143}Nd/^{144}Nd$ isotopic ratios for late Mesozoic volcanic rocks from the Hailar basin, NE China.

	Rb [ppm]	Sr [ppm]	$^{87}Rb/^{86}Sr$	$^{87}Sr/^{86}Sr$ (m.)	$^{87}Sr/^{86}Sr_{(t)}$	Sm [ppm]	Nd [ppm]	$^{147}Sm/^{144}Nd$ (m.)	$^{143}Nd/^{144}Nd$ (m.)	T_{DM}[a] [Ga]	$\varepsilon_{Nd(t)}$[b]
Basaltic trachyandesite											
FK10-98	66.7	757	0.255	0.705910 ± 40	0.70533	12.08	66.14	0.1104	0.512570 ± 20	–	0.2
FK10-99	67.1	716	0.271	0.706293 ± 30	0.70568	12.27	66.84	0.1110	0.512561 ± 20	–	0.0
FK10-96	99.9	693	0.417	0.706444 ± 50	0.70549	12.41	67.18	0.1117	0.512616 ± 20	–	1.1
FK10-97	86.6	424	0.592	0.706976 ± 20	0.70563	10.80	58.64	0.1113	0.512564 ± 20	–	0.1
FK10-100	92.7	651	0.412	0.706530 ± 30	0.70559	8.422	44.31	0.1149	0.512581 ± 20	–	0.3
FK10-101	30.3	736	0.119	0.705452 ± 30	0.70518	7.798	38.38	0.1228	0.512646 ± 10	–	1.5
FK10-78	60.1	799	0.218	0.705677 ± 30	0.70518	11.40	64.87	0.1062	0.512648 ± 10	–	1.8
FK10-79	59.1	773	0.221	0.705485 ± 30	0.70498	10.90	61.17	0.1077	0.512668 ± 20	–	2.2
FK10-77	58.6	807	0.210	0.705568 ± 30	0.70509	11.42	65.13	0.1060	0.512646 ± 20	–	1.7
FK10-116	65.6	682	0.278	0.705511 ± 30	0.70496	8.759	49.97	0.1060	0.512659 ± 30	–	2.0
FK10-111	59.9	960	0.181	0.705888 ± 40	0.70553	8.142	48.15	0.1022	0.512603 ± 20	–	1.0
FK10-112	36.6	652	0.162	0.705122 ± 40	0.70480	6.218	29.81	0.1261	0.512742 ± 30	–	3.3
FK10-113	35.8	720	0.144	0.705613 ± 30	0.70533	–	–	–	–	–	–
Trachyte and I-type rhyodacite											
FK10-80	159	345	1.34	0.707500 ± 30	0.70499	9.795	56.82	0.1042	0.512684 ± 10	0.51	2.5
FK10-81	127	218	1.69	0.708158 ± 30	0.70499	11.10	65.34	0.1027	0.512695 ± 20	0.49	2.8
FK10-102	144	330	1.26	0.707420 ± 20	0.70505	5.094	25.00	0.1232	0.512713 ± 20	0.56	2.8
FK10-104	149	227	1.90	0.710168 ± 30	0.70661	7.339	37.61	0.1180	0.512627 ± 10	0.67	1.2
FK10-105	197	40.7	14.1	0.734680 ± 30	0.70828	3.533	21.99	0.0971	0.512553 ± 30	0.65	0.1
FK10-107	123	232	1.54	0.708270 ± 40	0.70556	5.476	30.29	0.1093	0.512717 ± 20	0.49	3.1
FK10-108	105	71.0	4.29	0.711184 ± 20	0.70363	4.901	28.85	0.1027	0.512701 ± 20	0.48	2.9
A-type rhyolite											
FK10-83	224	16.7	39.0	0.784319 ± 12	0.70882	9.734	40.38	0.1457	0.512742 ± 20	0.68	3.0
FK10-87	251	49.3	14.8	0.734773 ± 8	0.70671	9.724	41.17	0.1423	0.512756 ± 20	0.62	3.3
FK10-86	250	12.2	60.1	0.819918 ± 11	0.70531	10.63	45.80	0.1404	0.512734 ± 20	0.65	2.9
FK10-88	257	10.4	72.6	0.844261 ± 10	0.70649	6.743	32.73	0.1246	0.512711 ± 20	0.58	2.7
FK10-89	198	29.6	19.4	0.744399 ± 9	0.70785	8.161	34.93	0.1413	0.512730 ± 20	0.67	2.8
FK10-90	219	15.5	41.1	0.786341 ± 20	0.70695	10.04	46.20	0.1313	0.512731 ± 10	0.59	3.0
FK10-91	218	10.2	62.5	0.824482 ± 40	0.70639	10.94	50.03	0.1322	0.512735 ± 30	0.59	3.1
FK10-84	243	17.0	41.6	0.787952 ± 10	0.71516	8.844	37.90	0.1411	0.512726 ± 20	0.67	2.7
FK10-85	233	11.3	60.2	0.824936 ± 8	0.70847	9.805	41.12	0.1442	0.512732 ± 10	0.69	2.8

Errors of Sr and Nd isotopic ratios are within-run errors (2σ mean); m. = measured ratio, t = initial ratio; $\varepsilon_{Nd(t)}$ calculated with the parameter of Bouvier et al. (2008); the ε_{Nd} values in the mafic LREE-enriched rocks are not sensitive to age uncertainties; e.g., an age of up to 160 Ma would increase the ε_{Nd} values by only 0.4 units, which is similar to the error of the Nd isotopic ratios.

[a] Model-age calculation according to DePaolo (1981); Nd model-age concept is appropriate for felsic rocks and its detritus, not mantle-derived ones.

[b] Initial ratios are based on 125 Ma, the emplacement age of the felsic rocks of this study.

negative Nb-anomaly and a positive Pb-anomaly resulting in low arc-like Ce/Pb ratios of 7 to 10 in the samples (e.g., Miller et al., 1994; Taylor and McLennan, 1985; Tables 2, S3); high Th/Nb (>0.25) and high Th/La ratios

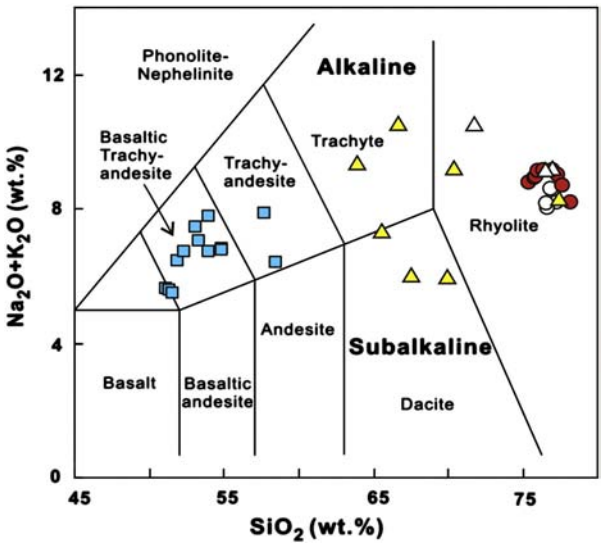

Fig. 3. SiO_2 vs. $Na_2O + K_2O$ concentrations of late Mesozoic volcanic rocks from the Hailar basin suggesting a bimodal composition (diagram of Le Bas et al., 1986). Squares: mafic volcanic rocks; triangles: felsic volcanic rocks; circles: A-type rhyolites (see Fig. 9 for felsite classification). Open triangles and circles are data from Ying et al. (2010) and Ge et al. (2001). Plotted data are anhydrous concentrations to facilitate comparison.

(~0.12) relative to MORB and OIB values (Fig. 5a) support a sedimentary component in the sources of the samples (e.g., Plank, 2005; Taylor and McLennan, 1985).

The Nd, Sr, and Pb isotopic compositions support the trace-element evidence for involvement of a sedimentary component. The initial $\varepsilon_{Nd(125\ Ma)}$ values of +0.4 to +3.4 in Fig. 6 are low relative to a model depleted asthenosphere of about +8 (DePaolo, 1981). Radiogenic $^{87}Sr/^{86}Sr$ ratios and high $^{207}Pb^{204}Pb$ ratios intermediate between depleted mantle and orogenic compositions (Fig. 7) indicate an old upper crustal component in the mantle source (Tables 3, S4). We have calculated ε_{Nd} values for the mafic rocks for 125 Ma, the age of the felsic rocks dated in this study although the mafic rocks are likely to be older. The initial ε_{Nd} value in these LREE-enriched mafic rocks are, however, not age-sensitive even assuming a possible maximum age up to 160 Ma, as can be seen by the small increase of ε_{Nd} by only 0.4 units. This discrepancy is similar to the analytical uncertainty and does not affect our interpretation.

As crustal magma contamination produces similar signatures in the contaminated magmas to those resulting from the melting of subduction-modified mantle sources, we need to address the possibility of crustal contamination. An important finding is the fact that our search for zircons in three mafic samples (FK 10–77, 78, 79) was not successful and by inference the presence of a significant amount of felsic crustal material is unlikely in these samples. The samples have ε_{Nd} values of +2.1 to +2.6 and show similar geochemical characteristics as the other samples so that we interpret these isotopic features as primary, mantle-derived signatures. Furthermore, ε_{Nd} values in the mafic rocks show no systematic variation with the degree of magma fractionation

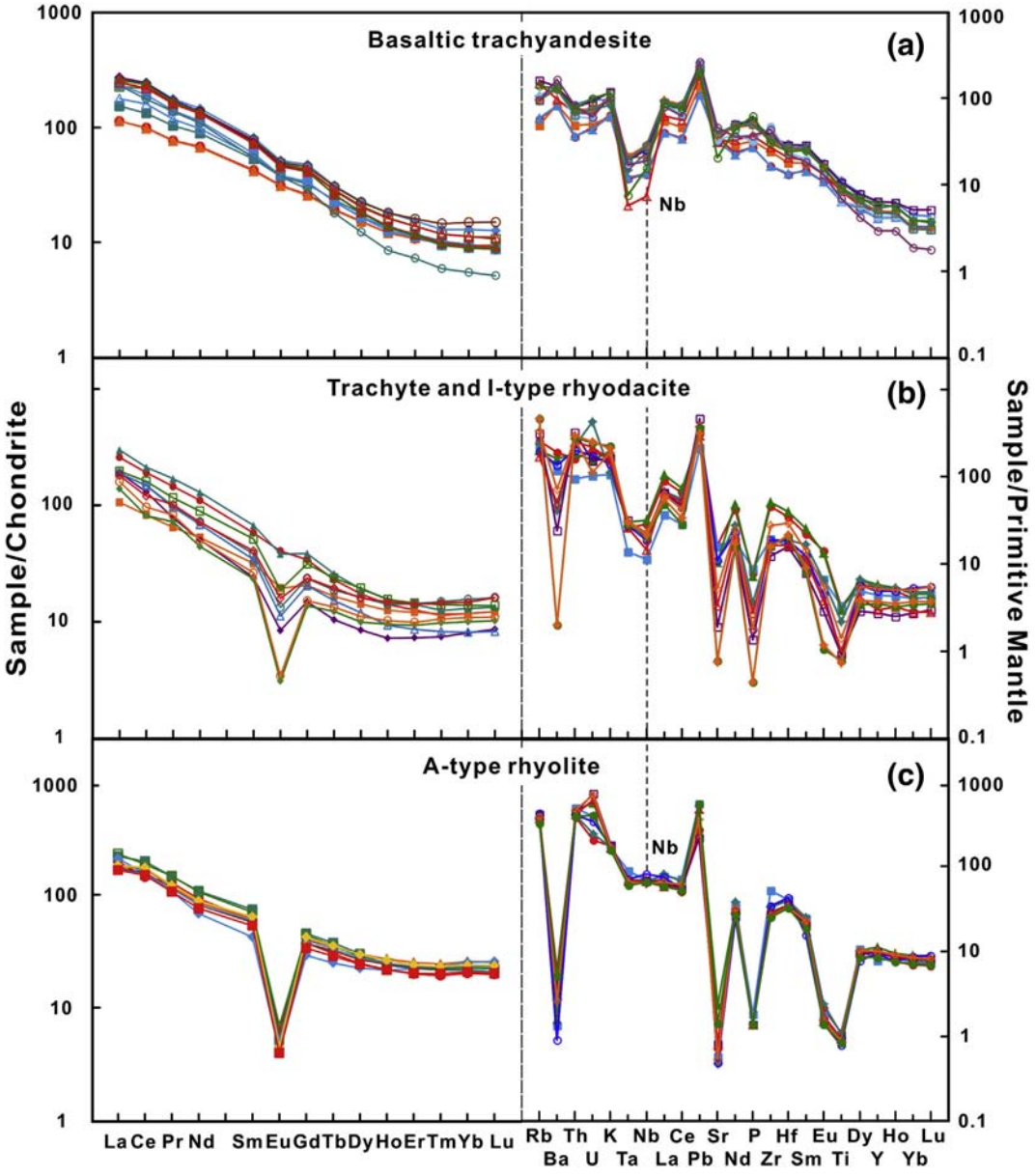

Fig. 4. Chondrite-normalized REE patterns and primitive mantle-normalized trace element patterns of late Mesozoic volcanic rocks from Hailar basin. Chondrite values are from Boynton (1984) and primitive-mantle values from Sun and McDonough (1989).

reflected in the Mg# (Table 3) and SiO_2 concentrations (Fig. 6b) so that we propose that the variations in ε_{Nd} values, $^{87}Sr/^{86}Sr$ ratios, and possibly Pb isotopes are similar to the mantle values.

In a La/Nb vs. Th/Nb diagram where 2-component mixing processes form linear data trends (Fig. 5a), the Hailar samples plot on a shallow data trend that is different from the near-vertical trend expected for assimilation of continental crust by a mantle-derived magma (Fig. 5a). The Hailar trend is compatible with the melting of a subduction-related marine sedimentary component with high La/Nb and Th/Nb and mantle material not modified by subduction, e.g., that of the MORB-OIB type. We conclude that the mafic samples of this study were not drastically affected by the assimilation of basement material during magma ponding and fractionation, and interpret their geochemical characteristics as those of the mantle source. However, reports of Neoproterozoic xenocrystic zircons in other samples from the Hailar basin (Zhang et al., 2008a) confirm the likelihood of magma contamination in intra-plate settings.

In Fig. 5b, the initial ε_{Nd} values of the mafic rocks are plotted vs. the La/Nb ratio as an index of the proportion of subduction-modified mantle material in the samples. It can be seen that the entire range of ε_{Nd} values from +3.4 to +0.4 exists in samples with similar arc-like La/Nb ratios of 3–4. This can be taken as evidence for an origin of the mafic volcanic rocks by the partial melting of an isotopically heterogeneous subduction-modified mantle. There is obviously no additional contribution from the asthenosphere without subduction characteristics, e.g., material from depth levels below that of slab dehydration residing at greater depth and higher pressures. This conclusion assumes that an upwelling asthenosphere not modified by slab dehydration would provide early in the melting process magmas with OIB characteristics from low-temperature melting enriched domains as has been shown for seamount volcanism from the flanks of ocean ridges (Batiza, 1982; Hegner and Tatsumoto, 1989; Zindler et al., 1984). Such magmas have low La/Nb of about 0.9 and high ε_{Nd} so that mixing with subduction-overprinted mantle material would produce compositions with low,

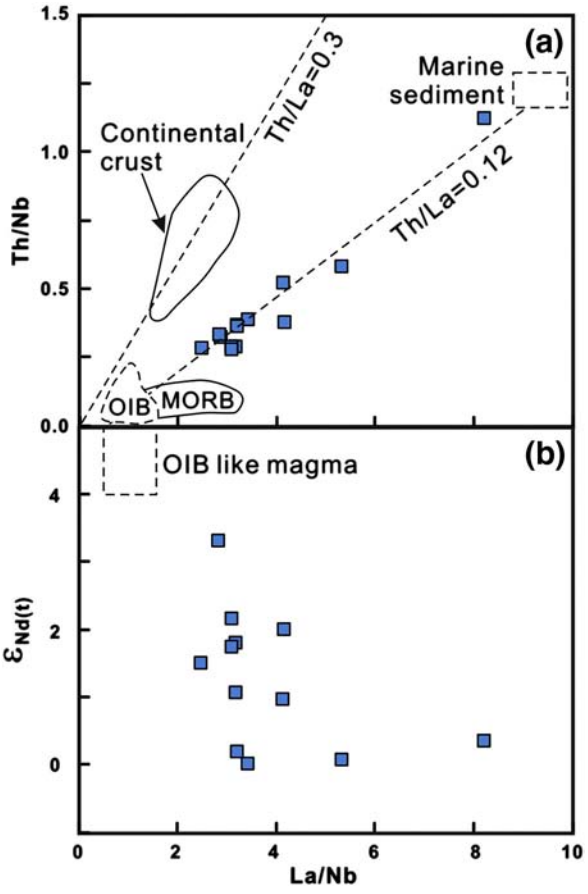

Fig. 5. (a) La/Nb vs. Th/Nb ratios of mafic late Mesozoic volcanic rocks from Hailar basin. High Th/Nb and La/Nb indicate subduction-modified arc-type mantle sources; field for "marine sediment" represents a possible composition of subducted sediment as can be inferred from the data trend (diagram modified after Plank, 2005). (b) La/Nb vs. initial ε_{Nd} values in mafic volcanic rocks showing a large range in ε_{Nd} values at similar La/Nb of 3–4 consistent with the melting of predominantly heterogenous subduction-modified mantle sources (see footnote Table 3 regarding age of initial ratios and Section 4.3 for discussion).

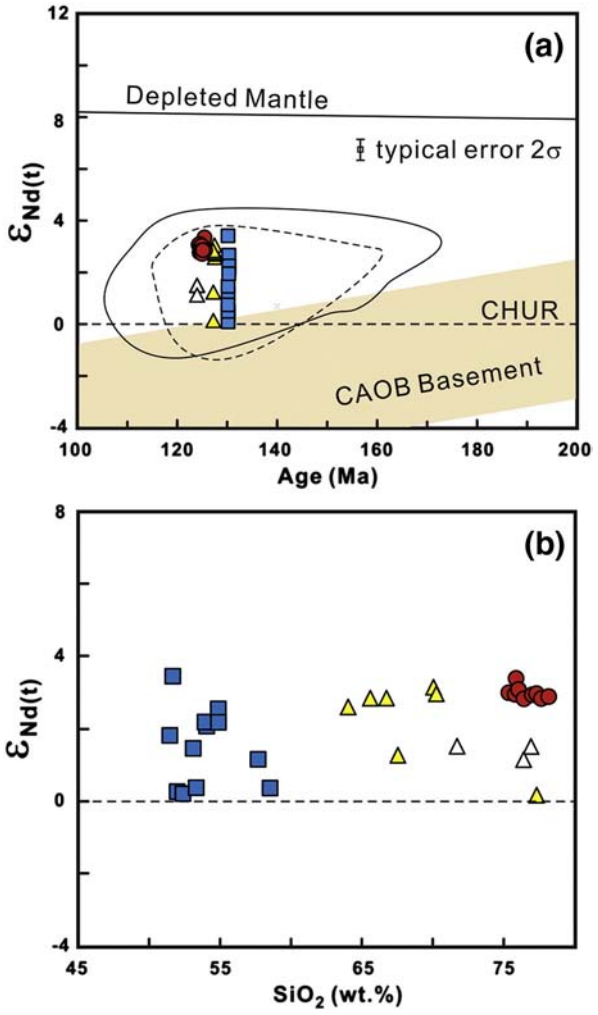

Fig. 6. (a) Nd isotopic evolution diagram for late Mesozoic volcanic rocks from the Hailar basin. Initial ε_{Nd} values for an assumed age of 125 Ma are plotted as a group for better visibility of data points. Data fields: solid line and stippled lines, late Mesozoic mafic and felsic rocks, respectively, from the Hailar basin (Fan et al., 2003; Zhang et al., 2008b); field in light gray, middle Carboniferous to middle Permian CAOB basement (data from Chen et al., 2009; Jian et al., 2008; Wu et al., 2000); depleted mantle line from DePaolo (1981). (b) SiO_2 concentrations vs. initial ε_{Nd} values showing isotopic similarity between mantle- and crust-derived felsic volcanic rocks, indicating a juvenile crustal source for the felsites.

non-arc-like, La/Nb ratios and the highest ε_{Nd} values in samples with the lowest La/Nb ratios, e.g., a negative correlation between these parameters. Such a relationship is not obvious in Fig. 5b, and so we conclude that a subduction-modified mantle represents the major source of the mafic extension-related magmatism at the Hailar basin.

4.3. Petrogenesis of felsic volcanic rocks

Drill cores from the Hailar basin show that lithospheric extension initiated bimodal mafic–felsic magmatism similar to that in other regions of an extending lithosphere in NE China (Xu et al., 2013) and worldwide (e.g., Christiansen and Lipman, 1972; Griffin et al., 2010). Without invoking very special magmatic processes (e.g., Brophy, 1991), the lack of intermediate rock types (Daly gap) and the large volume of felsic rocks relative to that of the mafic types in the Hailar region is consistent with an origin of felsic rocks by crustal partial melting. This feature is typical for settings of lithospheric extension and a consequence of magmatic underplating and crustal melting (e.g., Fountain, 1989; Huppert and Sparks, 1988). The origin of the felsic rocks from the Hailar basin has also been explained by fractionation of a mantle-derived magma (Fan et al., 2003) whereas Gou et al. (2013) proposed the partial melting of crustal sources. Magma unmixing processes mostly associated with anhydrous layered intrusions (see review of Charlier et al., 2013) can be precluded as the origin for mafic and felsic Hailar volcanic rocks also because of the overwhelming evidence for older felsic crust-derived xenocrystic zircons in the felsic volcanic rocks. They clearly indicate reworked older crustal protoliths as source material for Hailar felsites.

The data of our samples plotted in Harker diagrams (Figs. 4, 8) support a bimodal composition of the Hailar magmatism as can be inferred from the small number of intermediate compositions. SiO_2 vs. Al_2O_3 concentrations for mafic and felsic rocks (Fig. 8a) show unrelated magma fractionation trends resulting from plagioclase fractionation of compositionally different parental magma batches. The distinct P_2O_5 variation in mafic and felsic rock samples (Fig. 8b) are further evidence for unrelated magma fractionation processes. Finally, the enrichment of the LREE relative to the HREE during magma fractionation of the mafic volcanic rocks, as shown by the increasing La/Yb ratio with increasing SiO_2 (Fig. 8c), produces a compositional gap relative to the felsic rocks that cannot be reconciled with a common origin by crystal fractionation. We emphasize that the samples have different ages and probably represent magma batches belonging to different fractionating magma series. Nevertheless, we argue that the data trends reflect the principle magmatic processes in the Hailar basin and that the systematic differences for mafic and felsic rock series are due to fractionation of different parental magmas and not fractionation of a common parental magma.

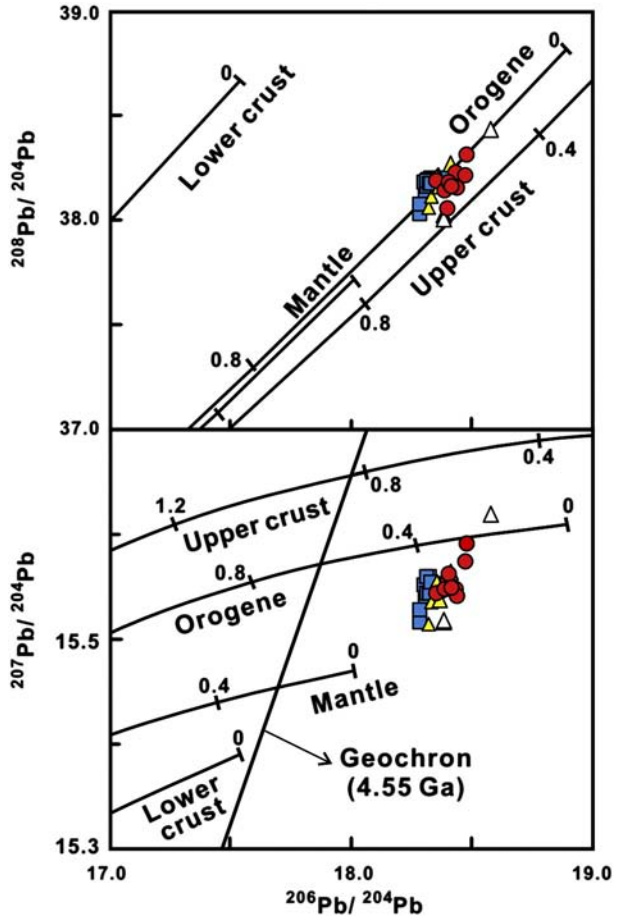

Fig. 7. Initial Pb isotopic compositions calculated for an age of 125 Ma for late Mesozoic mafic and felsic volcanic rocks from the Hailar basin. High $^{207}Pb/^{204}Pb$ ratios in the samples relative to the plumbotectonic model of Zartman and Doe (1981) indicate the melting of an old upper crustal component. The ticks on the curves indicate age intervals in Ga.

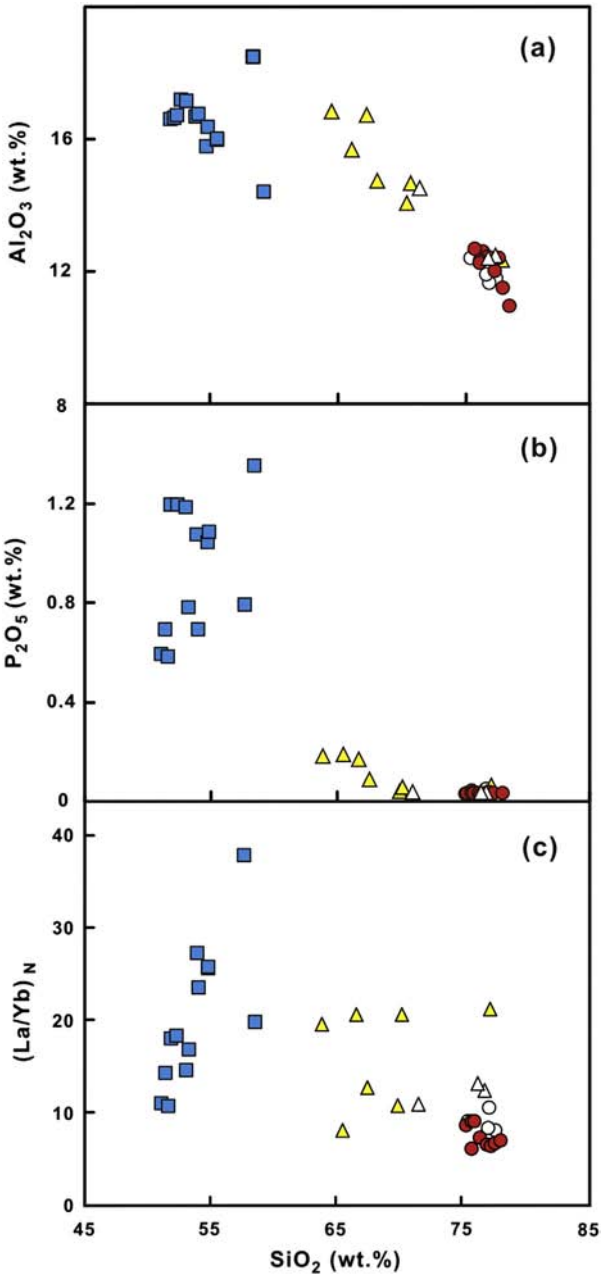

Fig. 8. Harker diagrams showing separate crystal fractionation trends for the mafic and felsic volcanic rocks of the Hailar basin. Although the mafic and felsic samples differ in age, precluding a comagmatic relationship among them, the Daly gap and fundamentally different magmatic trends suggest different parental magmas for felsic and mafic volcanic rocks. See Section 4.3 for discussion; symbols as in Fig. 3.

We conclude that the mafic and felsic rock assemblage of the Hailar basin was produced by melting processes in the upwelling upper mantle and lower crust, respectively.

Nd, Sr, and Pb isotopic ratios for the felsic rocks show heterogeneous crustal sources that are indistinguishable from those of the mafic volcanic rocks and different from the composition of the CAOB basement (Figs. 6, 7; Table 3; see Section 4.5 for discussion). Apparently, the felsic rocks were formed by the melting of a juvenile crustal source formed by underplating of mantle-derived material. Ga and Nb concentrations (Fig. 9a) show that crustal melting produced felsites of I- and A-type compositions (Whalen et al., 1987). A-type rhyolites represent a very rare rock-type in comparison to the abundant I-type felsites in the Hailar basin and apparently melting conditions leading to A-type compositions were not as widespread in the rifting crust as those forming the abundant I-type varieties.

I-type felsites of trachytic to rhyolitic composition show subparallel REE patterns with fractionated LREE and much less-fractionated, concave HREE patterns (Fig. 4b). The latter feature can be explained with residual and fractionating hornblende which occurs as a phenocryst in a thin section. Plagioclase control during melting and magma fractionation is indicated by variable Eu-anomalies. The A-type rhyolites have uniform REE patterns with similar Eu-anomalies, concave HREE patterns, and show less enrichment in the LREE relative to the HREE than the I-type rhyolites (Fig. 4c, Table 3). I-type trachyte and rhyolite samples show negative Nb-anomalies similar to those in mafic rocks and this anomaly is virtually absent in the A-type rhyolites. All felsic rock types have well-defined negative Ba, Sr, and Eu-anomalies due to extensive feldspar crystallization, and their negative P-anomalies indicate apatite fractionation and/or residual apatite in the case of felsic sources. The negative Ti-anomalies are probably due to crystallization of sphene, a ubiquitous phase in a thin section. The large positive Pb-anomalies and low crustal Ce/Pb ratios (Tables 2, S3) in combination with high $^{207}Pb/^{204}Pb$ ratios (Fig. 7) are consistent with sources enriched with hydrothermal/magmatic Pb and an ancient sedimentary component.

Although I- and A-type felsites overlap in age, the geochemical relationship between them suggests different sources and magmatic histories as described below. Using immobile Th and SiO_2 concentrations as magma fractionation indices (Fig. 9b), the I-type rhyolites show increasing Th concentrations with increasing degrees of fractionation. However, for a similar degree of magma fractionation, e.g., at 76 wt.% SiO_2, the A-type rhyolites, show a much higher Th concentration. This difference

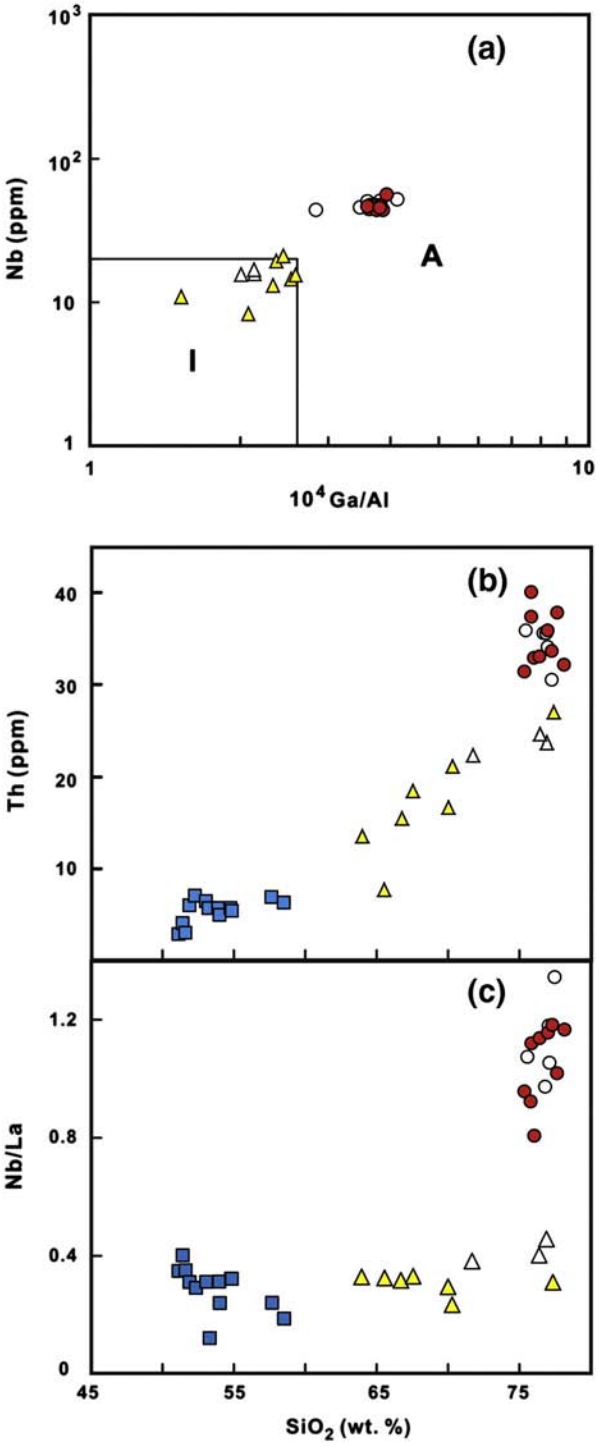

Fig. 9. Trace-element variation diagrams for late Mesozoic volcanic rocks from the Hailar basin. (a) Ga/Al ratios vs. Nb concentrations indicate felsic samples with A- and I-type affinities (diagram from Whalen et al., 1987); (b) SiO_2 vs. Th concentrations, and (c) SiO_2 concentrations vs. Nb/La ratios for felsic volcanic rocks suggest different origins for A- and I-type felsites. See Section 4.3 for discussion; symbols as in Fig. 3.

cannot be reconciled with an origin of the A-type rhyolites from the most fractionated I-type rhyolites. In Fig. 9c. it can be seen that I-type felsic volcanics have similar and large negative Nb-anomalies as in the mafic volcanic rocks, whereas the A-type rhyolites show only small (positive and negative) Nb anomalies. This difference exists for a similar degree of magma fractionation, e.g., at around 76 wt.% SiO_2. As there is no obvious process or mineral to account for the drastic decrease of the Nb anomaly in the A-type felsites, without changing the degree of magma fractionation, and thereby the SiO_2 content, we conclude that A- and I-type felsites were formed from different sources and by distinct magmatic processes as will be described in more detail below.

The difference in origin of A- and I-type felsites is further shown in Fig. 10a, where both rock types form subparallel and negatively correlated data trends. For a given La concentration, the A-type rhyolites have a higher Th/La ratio implying that both types of felsic rock series were derived from chemically different parental magma batches. For the I-type samples the importance of fractionation of plagioclase is well illustrated by the increasing negative Eu-anomaly with an increasing degree of magma fractionation, e.g., SiO_2 concentration (Fig. 10b). In Fig. 10c, it can be seen that in I- and A-type felsites the La concentrations, and by inference those of other LREE, decrease, with increasing SiO_2 concentrations and degree of magma fractionation. This trend can be explained with crystallization of apatite as is evident in Fig. 8b and the negative P-anomaly in the trace-element patterns (Fig. 4b, c). Due to the affinity of apatite for the LREE (Henderson, 1982; Prowatke and Klemme, 2006), its fractionation will deplete the magma in LREE and enrich less compatible Th (Prowatke and Klemme, 2006), thereby increasing the Th/La ratio and this effect can be seen in the data trends in Fig. 10a.

Apatite fractionation apparently has also controlled the magnitude of the Nb-anomaly in the A-type rhyolites as suggested by the data trend in Fig. 10d. The negative correlation between La and Nb/La is consistent with the inferred fractionation of apatite from the magma and the gradual disappearance of the anomaly (Nb/La ~1.1 signifies no anomaly). This trend can be explained with the removal of LREE in apatite whereas Nb behaves in a less compatible manner (Prowatke and Klemme, 2006). During the partial melting of felsic material, residual phosphate minerals would produce a similar effect and, in addition to its fractionation from the magma, would contribute to the elimination of the Nb-anomaly. We conclude that accessory apatite appears to be responsible for the high Nb/La ratios in the A-type felsites.

4.4. Melting of asthenospheric and lithospheric mantle during crustal extension

Geophysical data of the Hailar basin show at present a continental crust of about 40 km thickness underlain by almost 60 km of mantle lithosphere (An and Shi, 2006; Li et al., 2006). If all of the mantle lithosphere that had formed after the assembly of the CAOB had been removed by late Mesozoic magmatism, for which there is no geochemical evidence in the samples of this study, we can estimate that a maximum of about 60 km of lithospheric mantle was formed over the last 110 Ma since the end of basin formation. This age span is similar to that from completion of the CAOB until onset of late Mesozoic magmatism so that we suggest that a maximum of 60 km of lithospheric mantle (assuming similar geothermal gradients) was underlying the Hailar basin before the beginning of lithospheric extension and related magmatism. Assuming that the dehydration of subducting plates under the accreting arcs of the CAOB overprinted the upper mantle to depths of at least 150 km with fluids and melts from subducted sediment (e.g., Schmidt and Poli, 1998; Tatsumi and Kogiso, 2003; Tatsumi et al., 1986; not considering break-down of hydrous high-pressure phases at greater depths, e.g., Maruyama and Okamoto, 2007), it seems plausible that by late Mesozoic not all of the earlier subduction-modified mantle had been converted to mantle lithosphere and that a subduction-modified asthenosphere was underlying the thinning lithospheric mantle. It can be assumed that the upper mantle under the CAOB was geochemically zoned with a decreasing subduction-modification with depth possibly due to the mixing of depleted corner-flow material with a subduction modified mantle. For such a geochemically zoned mantle, it can be assumed that its uppermost portion had been converted to mantle lithosphere by the late Mesozoic. This mantle segment probably had an isotopic composition

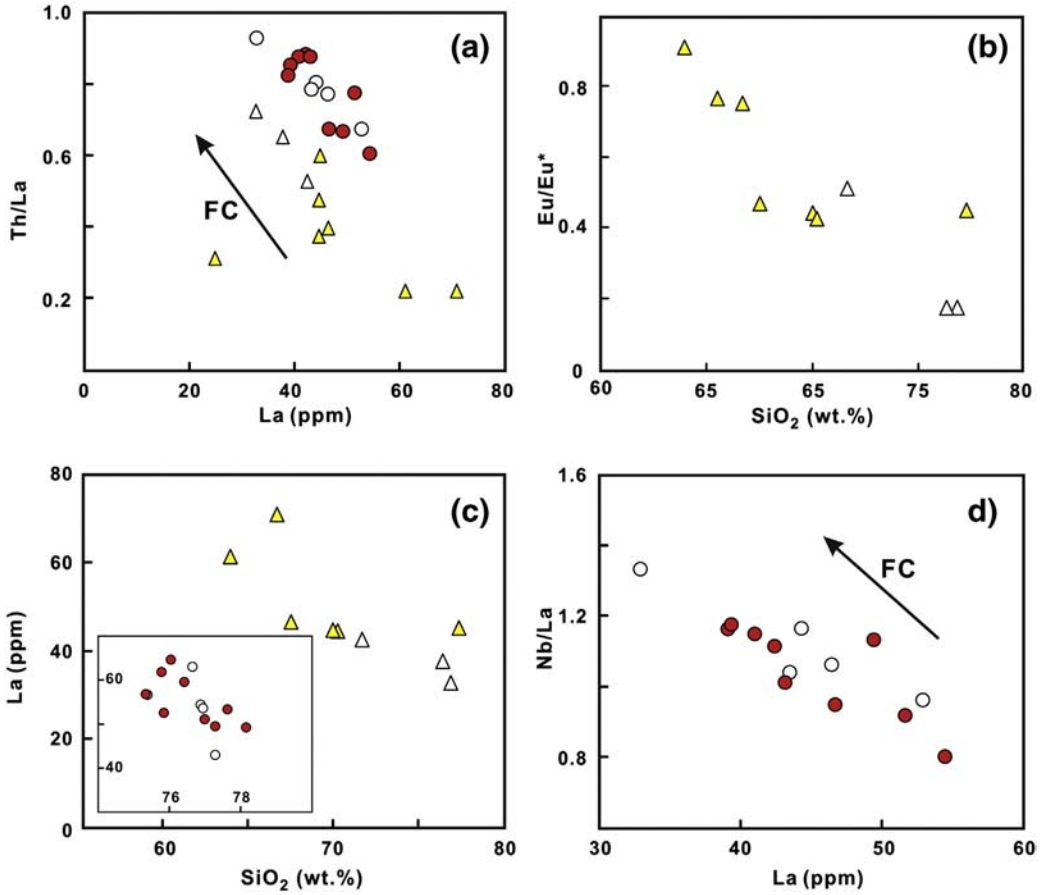

Fig. 10. Trace-element data for late Mesozoic I- and A-type felsic volcanic rocks from the Hailar region. (a) La concentrations vs. Th/La ratios for I- and A-type felsites, (b) SiO_2 concentrations vs. Eu/Eu* ratios for I-type felsites, (c) SiO_2 vs. La concentrations for I-type felsites, and, inset A-type rhyolites, and (d) La concentrations vs. Nb/La ratios for A-type rhyolites. The arrows indicate increasing fractional crystallization (FC) as inferred from SiO_2 as differentiation index (see Section 4.3 for discussion; symbols as in Fig. 3; for calculation of Eu/Eu* ratio see footnote of Table 2).

similar to the overall juvenile CAOB crust, because it represented its ultimate source.

It can be assumed that partial melting in such a geochemically zoned upper mantle would be initiated in the incompatible-element enriched low-T melting domains of the upwelling subduction-modified upper asthenosphere, rather than the cold lithospheric mantle portion. Contributions from the latter may have become important after the heating of its base by underplating asthenosphere-derived magmas and after the heating of the lithospheric mantle along magma conduits (e.g., Havlin et al., 2013; Turcotte, 1987). Yet, the importance of the melting of the lithospheric mantle under Hailar is documented in the negative K-anomaly in the mafic volcanic rocks that indicate a residual K-phase (amphibole, phlogopite) during partial melting. These phases are not stable in a hot convecting asthenosphere or an upwelling plume but in a cool and stagnant metasomatized mantle (e.g., Class and Goldstein, 1997). Magmas from the subduction-modified asthenosphere and the mantle lithosphere would show similar subduction features such as high La/Nb and low Ce/Pb ratios. However, it can be speculated that the Nd isotopic compositions of the magmas would differ with respect to the proportion of material from the lithospheric mantle vs. the subduction-modified asthenosphere. The uppermost portions of the former reservoir would be compositionally similar to overlying CAOB whereas magmas from a deeper subduction-modified upper asthenosphere would be expected to show higher ε_{Nd} values due to mixing with a depleted asthenosphere transported by corner-flow.

Using the geochemical data it can be concluded that the volcanic samples from the Hailar basin originated from a subduction-modified mantle (e.g., high La/Nb, low Ce/Pb ratios) containing subducted older sediment (e.g., high Th/Nb; radiogenic $^{207}Pb/^{204}Pb$ and $^{87}Sr/^{86}Sr$, and unradiogenic $^{143}Nd/^{144}Nd$). For addressing the question of the melting of the asthenosphere and lithospheric mantle sources we will resort to the geochemical background scenario described above and focus on ε_{Nd} values for which there is a large published data base. The field for ε_{Nd} values in Fig. 6a indicates the melting of overall similar mantle sources with compositions of +4 to −1 over a period of ca. 60 Ma of lithospheric extension at the Hailar region. The data plot in most cases above the data field of CAOB crust which we interpret as the composition of the uppermost mantle that had been converted into mantle lithosphere by the time when lithospheric extension took place. In our model we assume that the major source of magmatism was an upwelling and melting subduction-modified upper asthenosphere. This part of the mantle is clearly different from a typical depleted convecting asthenosphere with ε_{Nd} values of up to +8 (DePaolo, 1981). The data field for the younger rocks overlaps the field of the CAOB basement that according to our interpretations should be similar to the composition of the upper lithospheric mantle. Consequently we infer for these samples the melting of predominantly old subduction-modified lithospheric mantle. Melting and assimilation of lithospheric mantle would become important only after sufficient heating by asthenosphere-derived magmas ponding at the base and intruding the mantle lithosphere. On the other hand, ongoing crustal magma underplating in the course of magmatism would increase also the likelihood of crustal magma contamination. This process would be difficult to distinguish from lithospheric mantle input with the geochemical and isotopic data at hand. The geochemical evidence for the melting of subduction-modified mantle sources with a similar Nd isotopic composition during basin development at Hailar and Songliao to the east (our unpubl. data) cannot be easily explained with a model of a delaminating lithospheric

mantle as a reason for late Mesozoic volcanism (Wang et al., 2006). This concept implies the melting of increasingly larger proportions of the depleted asthenospheric mantle with time, e.g., the most depleted sources should be best developed in the youngest rocks, e.g., of ca. 110 Ma, when the replacement of the lithospheric mantle under Hailar should have been most advanced. In Fig. 6a, the ε_{Nd} values of late Mesozoic volcanic rocks apparently do not increase in the period from 160 Ma to 110 Ma; a maximum value of about +4, relative to a model depleted asthenosphere of +8 (DePaolo, 1981) is not exceeded. The Nd isotopic evidence for the melting of similar depleted mantle material, yet an increasing involvement of an enriched mantle lithosphere with an ongoing lithospheric extension, favors a model of an extending lithosphere where low-temperature melting subduction-modified domains in the upwelling asthenosphere are preferentially melted and the lithospheric mantle becomes heated and increases in importance as a magma source with time.

4.5. Reworking and rejuvenation of lower crust during lithospheric extension

For regions of lithospheric thinning, extensive magmatic underplating of crust by mantle-derived magmas is invoked due to the high density contrast (e.g., Hanson, 1981; Herzberg et al., 1983; Stolper and Walker, 1980). The mantle-derived basaltic magmas transport heat into the lower crust causing its melting and a complex interplay of magmatic processes (e.g., Fountain, 1989; Huppert and Sparks, 1988), collectively termed as MASH (melting, assimilation, storage, homogenization; Hildreth and Moorbath, 1988). The ponding mantle-derived magmas are prone to contamination by crust (e.g., Bergantz, 1989; Cox and Hawkesworth, 1985; Ewart et al., 1980; Hegner et al., 1984; Moorbath and Bell, 1965).

The lack of geochemical variation among our mafic rock samples makes it difficult to identify crustal assimilation but the fact that three of the basaltic trachyandesite samples did not yield any zircons in addition to the lacking geochemical and isotopic evidence for magma contamination (see discussion in Section 4.2) suggests that this process was not important for the samples of this study. However, xenocrystic zircons with ages of 480 and 780 Ma in other mafic rocks from the Hailar basin clearly show that assimilation of CAOB basement was important in other samples (Zhang et al., 2008a). The felsic rocks of the Hailar basin provide an interesting view of the response of the crust to magmatic underplating and melting. The age spectrum for xenocrystic and magmatic zircons of this study show that crustal protoliths were melted during lithospheric rifting from ca. 158 Ma to 125 Ma, with an apparent peak from 140 to 130 Ma as inferred from the large number of xenocrystic zircons of this age. The predominance of 140–130 Ma old zircons coincides with the voluminous felsic volcanism of the upper the Shangkuli Formation (Xu et al., 2013; Zhang et al., 2010).

We are able to address some details of crustal melting processes with the data from the I- and A-type felsites. The I-type felsites have negative Nb-anomalies and isotopic compositions overlapping those for the mafic volcanic rocks (Figs. 6b, 7). The geochemical and isotopic similarity with the mafic rocks, the evidence for an origin by the partial melting of crust (e.g., Daly gap and distinct magma fractionation), and isotopic compositions distinct from the CAOB basement (Fig. 6a), led us to propose the melting of predominantly underplated juvenile mantle-derived material with a component from juvenile felsic rocks as required by the presence of inherited zircons in the I-type sample of this study. The lack of xenocrystic zircon ages older than ca. 160 Ma precludes reworking of CAOB crust. U–Pb zircon ages reported for other I-type felsites from the Hailar region document deposition from ca. 158 Ma until 110 Ma, yet constituting the major rock type of the upper volcanic sequence. Apparently crustal heating and melting lagged behind mantle melting as can be inferred from the relationship of older predominantly basaltic rocks overlain by predominantly felsic volcanic rocks with subordinate basalts.

The abundant xenocrystic zircons and their age spectra and ε_{Nd} values of the A-type rhyolites indicate that the melting of juvenile felsic crustal sources was also important during lithospheric extension although at a much smaller scale than the melting of mafic protoliths. Absence of xenocrystic zircons from the CAOB basement and Nd isotopes support an ultimately juvenile mantle-derived source for the A-type rhyolites and we suggest I-type felsic material as the source. Chemical variation trends for the A-type rhyolite show an important role of apatite during magma fractionation and we propose that residual apatite in their felsic protoliths may have profoundly contributed to their high Nb/La ratios, a characteristic feature of A-type rhyolites (Collins et al., 1982; Martin et al., 1994; Whalen et al., 1987, 1996).

We conclude that the bimodal Hailar volcanic suite reflects a history of basin development with continuous crustal underplating by mantle-derived magmas leading to heating and extensive reworking of the lower crust. Eruption of large volumes of felsic material during the final stage of crustal extension may be due to the fact that the lower crust had reached temperatures sufficiently high for large-scale melting before extension ceased. The Nd isotopic data show that extension of the lithosphere led to significant rejuvenation of the lower crust which was further processed by partial melting to mafic cumulates and felsic material.

5. Conclusions

1. Geochemical characteristics of basaltic rocks from the late Mesozoic Hailar basin are consistent with the melting of upwelling old subduction-modified mantle including mantle lithosphere; depleted asthenosphere was not important as magma source during lithospheric extension.
2. U–Pb zircon ages of I- and rare A-type rhyolites, range from ca. 158 to 125 Ma overlapping the time of magmatism in the Hailar basin and indicate protracted reworking of juvenile felsic lower crust probably due to ongoing heating by underplating mantle-derived magmas.
3. Geochemical and isotopic evidence for the I-type felsic rocks support the partial melting of predominantly juvenile mantle-derived crustal protoliths whereas the A-type rhyolites can be related to the melting of predominantly I-type felsic lower crust, with residual and fractionating apatite controlling the Nb anomaly.
4. The temporal persistence of subduction-related geochemical characteristics in late Mesozoic mantle-derived rocks in NE China is consistent with a passively thinning lithosphere with coupled mantle and crust due to a retreating Paleo-Pacific trench.

Supplementary data to this article can be found online at http://dx.doi.org/10.1016/j.lithos.2013.12.009.

Acknowledgements

This study was financially supported by the Ministry of Science and Technology of China (grant 2009CB219305) and the National Nature Science Foundation of China (grants 41090372 and 40973042). The paper was written during a visit of Li S.-Q. to Munich University financed by the LMU-China Scholarship Council Program. Hou Z.-H., Xiao P., and He J.-F. are thanked for help during isotopic analyses. We gratefully acknowledge the help and constructive comments of Editor A. Kerr, M.F. Zhou, and an anonymous reviewer.

References

A, M.N., Zhang, F.Q., Yang, S.F., Chen, H.L., Batt, G.E., Sun, M.D., Meng, Q.A., Zhu, D.F., Cao, R.C., Li, J.S., 2013. Early Cretaceous provenance change in the southern Hailar Basin, northeastern China and its implication for basin evolution. Cretaceous Research 40, 21–42.

An, M., Shi, Y., 2006. Lithospheric thickness of the Chinese continent. Physics of the Earth and Planetary Interiors 159, 257–266.

Andersen, T., 2002. Correction of common lead in U–Pb analyses that do not report Pb-204. Chemical Geology 192, 59–79.
Bailey, D.K., 1974. Continental rifting and alkaline magmatism. In: Sorensen, H. (Ed.), The Alkaline Rocks. Wiley, pp. 148–159.
Batiza, R., 1982. Abundances, distribution and sizes of volcanoes in the Pacific ocean and implications for the origin of non-hotspot volcanoes. Earth and Planetary Science Letters 60, 195–206.
Bergantz, G.W., 1989. Underplating and partial melting: implications for melt generation and extraction. Science 245, 1093–1095.
Bouvier, A., Vervoort, J.D., Patchett, P.J., 2008. The Lu–Hf and Sm–Nd isotopic composition of CHUR: constraints from unequilibrated chondrites and implications for the bulk composition of terrestrial planets. Earth and Planetary Science Letters 273, 48–57.
Boynton, W.V., 1984. Geochemistry of the rare earth elements: meteorite studies. In: Henderson, P. (Ed.), Rare Earth Element Geochemistry. Elsevier, Amsterdam, pp. 63–114.
Brophy, J.G., 1991. Composition gaps, critical crystallinity, and fractional crystallization in orogenic (calc-alkaline) magmatic systems. Contributions to Mineralogy and Petrology 109, 173–182.
Charlier, B., Namur, O., Grove, T.L., 2013. Compositional and kinetic controls on liquid immiscibility in ferrobasalt–rhyolite volcanic and plutonic series. Geochimica et Cosmochimica Acta 113, 79–93.
Chen, F., Hegner, E., Todt, W., 2000. Zircon ages and Nd isotopic and chemical compositions of orthogneisses from the Black Forest, Germany: evidence for a Cambrian magmatic arc. International Journal of Earth Sciences 88, 791–802.
Chen, Z.G., Zhang, L.C., Zhou, X.H., Wan, B., Ying, J.F., Wang, F., 2006. Geochronology and geochemical characteristics of volcanic rocks section in Manzhouli Xinyouqi, Inner-Mongolia (in Chinese with English abstract). Acta Petrologica Sinica 22, 2971–2986.
Chen, B., Jahn, B.M., Tian, W., 2009. Evolution of the Solonker suture zone: constraints from zircon U–Pb ages, Hf isotopic ratios and whole-rock Nd–Sr isotopic compositions of subduction- and collision-related magmas and forearc sediments. Journal of Asian Earth Sciences 34, 245–257.
Christiansen, R.L., Lipman, P.W., 1972. Cenozoic volcanism and plate-tectonic evolution of the western United States. II. Late Cenozoic. Philosophical Transactions of the Royal Society of London. Series A Mathematical and Physical Sciences 271, 249–284.
Class, C., Goldstein, S.L., 1997. Plume–lithosphere interactions in the oceanic basins: constraints from the source mineralogy. Earth and Planetary Science Letters 150, 245–260.
Collins, W.J., Beams, S.D., White, A.J.R., Chappell, B.W., 1982. Nature and origin of a-type granites with particular reference to southeastern Australia. Contributions to Mineralogy and Petrology 80, 189–200.
Cox, K.G., Hawkesworth, C.J., 1985. Geochemical stratigraphy of the Deccan Traps at Mahabaleshwar, western Ghats, India, with implications for open system magmatic processes. Journal of Petrology 26, 355–377.
Daoudene, Y., Ruffet, G., Cocherie, A., Ledru, P., Gapais, D., 2009. The Ereendavaa Range (north-eastern Mongolia): an additional argument for Mesozoic extension throughout eastern Asia. International Journal of Earth Sciences 98, 1381–1393.
DePaolo, D.J., 1981. A neodymium and strontium isotopic study of the Mesozoic calc-alkaline granitic batholiths of the Sierra-Nevada and Peninsular Ranges, California. Journal of Geophysical Research 86, 470–488.
Dobretsov, N.L., Vernikovsky, V.A., 2001. Mantle plumes and their geologic manifestations. International Geology Review 43, 771–787.
Dobretsov, N.L., Berzin, N.A., Buslov, M.M., 1995. Opening and tectonic evolution of the Paleo-Asian Ocean. International Geology Review 37, 335–360.
Ewart, A., Baxter, K., Ross, J.A., 1980. The petrology and petrogenesis of the Tertiary anorogenic mafic lavas of southern and central Queensland, Australia—possible implications for crustal thickening. Contributions to Mineralogy and Petrology 75, 129–152.
Fan, W.M., Guo, F., Wang, Y.J., Lin, G., 2003. Late Mesozoic calc-alkaline volcanism of post-orogenic extension in the northern Da Hinggan Mountains, northeastern China. Journal of Volcanology and Geothermal Research 121, 115–135.
Faure, M., Natalin, B., 1992. The geodynamic evolution of the eastern Eurasian margin in Mesozoic times. Tectonophysics 208, 397–411.
Fountain, D.M., 1989. Growth and modification of lower continental crust in extended terrains: the role of extension and magmatic underplating. In: Mereu, R.F., Mueller, S., Fountain, D.M. (Eds.), Properties and Processes of Earth's Lower Crust, Am. Geophys. Union Monogr. 51. IUGG, vol. 6. American Geophysical Union, Washington, DC, pp. 287–299.
Gao, Y.Q., Liu, L., Hu, W.X., 2009. Petrology and isotopic geochemistry of dawsonite bearing sandstones in Hailar Basin, northeastern China. Applied Geochemistry 24, 1724–1738.
Ge, W.C., Lin, Q., Sun, D.Y., Wu, F.Y., Won, C.K., Lee, M.W., Jin, M.S., Yun, S.H., 1999. Geochemical characteristics of the Mesozoic basalts in Da Hinggan Ling: evidence of the mantle–crust interaction (in Chinese with English abstract). Acta Petrologica Sinica 15, 397–407.
Ge, W.C., Li, X.H., Lin, Q., Sun, D.Y., Wu, F.Y., Yun, S.H., 2001. Geochemistry of early Cretaceous alkaline rhyolites from Hulun Lake, Da Xing'an Ling and its tectonic implications (in Chinese with English abstract). Scientia Geologica Sinica 36, 176–183.
Gou, J., Sun, D.Y., Liu, Y.J., Ren, Y.S., Zhao, Z.H., Liu, X.M., 2013. Geochronology, petrogenesis, and tectonic setting of Mesozoic volcanic rocks, southern Manzhouli area, Inner Mongolia. International Geology Review 55, 1–20.
Graham, S.A., Cope, T., Johnson, C.L., Ritts, B., 2012. Sedimentary basins of the late Mesozoic extensional domain of China and Mongolia. In: Roberts, D.G., Bally, A.W. (Eds.), Phanerozoic Rift Systems and Sedimentary Basins. Elsevier, Amsterdam, The Netherlands, pp. 443–461.
Griffin, W.R., Foland, K.A., Stern, R.J., Leybourne, M.I., 2010. Geochronology of bimodal alkaline volcanism in the Balcones Igneous Province, Texas: implications for Cretaceous intraplate magmatism in the northern Gulf of Mexico magmatic zone. The Journal of Geology 118, 1–21.
Guo, Z., Wilson, M., Liu, J., Mao, Q., 2006. Post-collisional, potassic and ultrapotassic magmatism of the northern Tibetan Plateau: constraints on characteristics of the mantle source, geodynamic setting and uplift mechanisms. Journal of Petrology 47, 1177–1220.
Guo, F., Fan, W., Gao, X., Li, C., Miao, L., Zhao, L., Li, H., 2010. Sr–Nd–Pb isotope mapping of Mesozoic igneous rocks in NE China: constraints on tectonic framework and Phanerozoic crustal growth. Lithos 120, 563–578.
Hanson, G.N., 1981. Geochemical constraints on the evolution of the early continental crust. Philosophical Transactions of the Royal Society of London. Series A Mathematical and Physical Sciences 301, 423–442.
Havlin, C., Parmentier, E.M., Hirth, G., 2013. Dike propagation driven by melt accumulation at the lithosphere–asthenosphere boundary. Earth and Planetary Science Letters. http://dx.doi.org/10.1016/j.epsl.2013.06.010.
He, B., Xu, Y.G., Huang, X.L., Luo, Z.Y., Shi, Y.R., Yang, Q.J., Yu, S.Y., 2007. Age and duration of the Emeishan flood volcanism, SW China: geochemistry and SHRIMP zircon U–Pb dating of silicic ignimbrites, post-volcanic Xuanwei Formation and clay tuff at the Chaotian section. Earth and Planetary Science Letters 255, 306–323.
Hegner, E., Tatsumoto, M., 1989. Pb, Sr and Nd isotopes in seamount basalts from the Juan de Fuca Ridge and Kodiak–Bowie seamount chain, northeast Pacific. Journal Geophysical Research 94, 17839–17846.
Hegner, E., Kröner, A., Hofmann, A.W., 1984. Age and isotope geochemistry of the Archaean Pongola and Usushwana suites in Swaziland, southern Africa: a case for crustal contamination of mantle-derived magma. Earth and Planetary Science Letters 70, 267–279.
Hegner, E., Walter, H.J., Satir, M., 1995. Pb–Sr–Nd isotopic compositions and trace element geochemistry of megacrysts and melilitites from the Tertiary Urach volcanic field: source composition of small volume melts under SW Germany. Contributions to Mineralogy and Petrology 122, 322–335.
Henderson, P., 1982. Inorganic Geochemistry. Pergamon, Oxford.
Herzberg, C.T., Fyfe, W.S., Carr, M.J., 1983. Density constraints on the formation of the continental Moho and crust. Contributions to Mineralogy and Petrology 84, 1–5.
Hildreth, W., Moorbath, S., 1988. Crustal contributions to arc magmatism in the Andes of central Chile. Contributions to Mineralogy and Petrology 98, 455–489.
Hoskin, P.W., Schaltegger, U., 2003. The composition of zircon and igneous and metamorphic petrogenesis. Reviews in Mineralogy and Geochemistry 53, 27–62.
Hou, Z.H., Wang, C.Z., 2007. Determination of 35 trace elements in geological samples by inductively coupled plasma mass spectrometry (in Chinese with English abstract). Journal of University of Science and Technology of China 37, 940–944.
Hou, W.R., Nie, F.J., Jiang, S.H., Bai, D.M., Liu, Y., Yun, F., Liu, Y.F., 2010. The geology and ore-forming mechanism of the Tsagaan Suvarga large-size Cu–Mo porphyry deposit in Mongolia (in Chinese with English abstract). Acta Geoscientica Sinica 31, 307–320.
Huppert, H.E., Sparks, R.S.J., 1988. The generation of granitic magmas by intrusion of basalt into continental crust. Journal of Petrology 29, 599–624.
IMBGMR (Inner Mongolian Bureau of Geology and Mineral Resources), 1991. Regional Geology of Inner Mongolian Automo (in Chinese with English summary). Geological Publishing House, Beijing.
Jian, P., Liu, D.Y., Kröner, A., Windley, B.F., Shi, Y.R., Zhang, F.Q., Shi, G., Miao, L.C., Zhang, W., Zhang, Q., Zhang, L., Ren, J., 2008. Time scale of an early to mid-Paleozoic orogenic cycle of the long-lived Central Asian Orogenic Belt, Inner Mongolia of China: implications for continental growth. Lithos 101, 233–259.
Le Bas, M.J., Le Maitre, R.W., Streckeisen, A., Zanettin, B., 1986. A chemical classification of volcanic-rocks based on the total alkali silica diagram. Journal of Petrology 27, 745–750.
Li, J., Shu, L.S., 2002. Mesozoic–Cenozoic tectonic features and evolution of the Songliao Basin, NE China (in Chinese with English abstract). Journal of Nanjing University (Natural Science) 38, 525–531.
Li, S., Mooney, W.D., Fan, J., 2006. Crustal structure of mainland China from deep seismic sounding data. Tectonophysics 420, 239–252.
Li, S.Q., Chen, F., Siebel, W., Wu, J.D., Zhu, X.Y., Shan, X.L., Sun, X.M., 2012. Late Mesozoic tectonic evolution of the Songliao Basin, NE China: evidence from detrital zircon ages and Sr–Nd isotopes. Gondwana Research 22, 943–955.
Lin, Q., Ge, W.C., Sun, D.Y., Wu, F.Y., Won, C.K., Lee, M.W., Yun, S.H., Jin, M.S., Min, K.D., Kwon, C.S., 2000. Genetic relationships between two types of Mesozoic rhyolite and basalts in Great Xingan Ridge (in Chinese with English abstract). Journal of Changchun University of Science and Technology 30, 322–328.
Lin, Q., Ge, W.C., Cao, L., Sun, D.Y., Lim, K.G., 2003. Geochemistry of Mesozoic volcanic rocks in Da Hinggan Ling: the bimodal volcanic rocks (in Chinese with English abstract). Geochimica 32, 208–222.
Liu, X., Gao, S., Diwu, C., Yuan, H., Hu, Z., 2007. Simultaneous in-situ determination of U–Pb age and trace elements in zircon by LA–ICP-MS in 20 μm spot size. Chinese Science Bulletin 52, 1257–1264.
Ludwig, K.R., 2003. ISOPLOT 3: A Geochronological Toolkit for Microsoft Excel, 4. Geochronology Centre Special Publication, Berkeley 74.
Luo, W., Zhang, Z., Hou, T., Wang, M., 2013. Geochronology–geochemistry of the Cida bimodal intrusive complex, central Emeishan large igneous province, southwest China: petrogenesis and plume–lithosphere interaction. International Geology Review 55, 88–114.
Luo, W., Zhang, Z., Santosh, M., Hou, T., Huang, H., Zhu, J., Wang, X., Fu, X., 2014. Petrology and geochemistry of Permian mafic–ultramafic intrusions in the Emeishan large igneous province, SW China: insight into the ore potential. Ore Geology Reviews 56, 258–275.
Martin, H., Bonin, B., Capdevila, R., Jahn, B.M., Lameyre, J., Wang, Y., 1994. The Kuiqi peralkaline granitic complex (SE China): petrology and geochemistry. Journal of Petrology 35, 983–1015.
Maruyama, S., Okamoto, K., 2007. Water transportation from the subducting slab into the mantle transition zone. Gondwana Research 11, 148–165.

Meng, Q.R., 2003. What drove late Mesozoic extension of the northern China–Mongolia tract? Tectonophysics 369, 155–174.
Meng, E., Xu, W.L., Yang, D.B., Qiu, K.F., Li, C.H., Zhu, H.T., 2011. Zircon U–Pb chronology, geochemistry of Mesozoic volcanic rocks from the Lingquan Basin in Manzhouli area, and its tectonic implications (in Chinese with English abstract). Acta Petrologica Sinica 27, 1209–1226.
Meng, Q.A., Wan, C., Zhu, D., Zhang, Y., Ge, W., Wu, F., 2013. Age assignment and geological significance of the "Budate Group" in the Hailar Basin. Science China Earth Sciences 56, 1–10.
Miller, D.M., Goldstein, S.L., Langmuir, C.H., 1994. Cerium/lead and lead isotope ratios in arc magmas and the enrichment of lead in the continents. Nature 368, 514–519.
Moorbath, S., Bell, J.D., 1965. Strontium isotope abundance studies and rubidium–strontium age determinations on Tertiary igneous rocks from the Isle of Skye North–West Scotland. Journal of Petrology 6, 37–66.
Plank, T., 2005. Constraints from thorium/lanthanum on sediment recycling at subduction zones and the evolution of the continents. Journal of Petrology 46, 921–944.
Prowatke, S., Klemme, S., 2006. Trace element partitioning between apatite and silicate melts. Geochimica et Cosmochimica Acta 70, 4513–4527.
Ren, J.Y., Tamaki, K., Li, S.T., Zhang, J.X., 2002. Late Mesozoic and Cenozoic rifting and its dynamic setting in eastern China and adjacent areas. Tectonophysics 344, 175–205.
Ritts, B.D., Darby, B.J., Cope, T., 2001. Early Jurassic extensional basin formation in the Daqing Shan segment of the Yinshan belt, northern North China Block, Inner Mongolia. Tectonophysics 339, 239–258.
Schmidt, M.W., Poli, S., 1998. Experimentally based water budgets for dehydrating slabs and consequences for arc magma generation. Earth and Planetary Science Letters 163, 361–379.
Sengör, A.M.C., Natalin, B.A., Burtman, V.S., 1993. Evolution of the Altaid tectonic collage and Paleozoic crustal growth in Eurasia. Nature 364, 299–307.
Stolper, E., Walker, D., 1980. Melt density and the average composition of basalt. Contributions to Mineralogy and Petrology 74, 7–12.
Sun, S., McDonough, W.F., 1989. Chemical and isotopic systematics of oceanic basalts: implications for mantle composition and processes. In: Saunders, A.D., Norry, M.J. (Eds.), Magmatism in the Ocean Basins. Special Publication, 42. Geological Society, London, pp. 313–345.
Sun, M.D., Chen, H.L., Zhang, F.Q., Wilde, S.A., Dong, C.W., Yang, S.F., 2013. A 100 Ma bimodal composite dyke complex in the Jiamusi Block, NE China: an indication for lithospheric extension driven by Paleo-Pacific roll-back. Lithos. http://dx.doi.org/10.1016/j.lithos.2012.11.021.
Tatsumi, Y., Kogiso, T., 2003. The subduction factory: its role in the evolution of the Earth's crust and mantle. Geological Society, London, Special Publications 219, 55–80.
Tatsumi, Y., Hamilton, D.L., Nesbitt, R.W., 1986. Chemical characteristics of fluid phase released from a subducted lithosphere and origin of arc magmas: evidence from high-pressure experiments and natural rocks. Journal of Volcanology and Geothermal Research 29, 293–309.
Taylor, S.R., McLennan, S.M., 1985. The Continental Crust: Its Composition and Evolution. Blackwell Scientific Publications, Oxford.
Tomurtogoo, O., Windley, B.F., Kröner, A., Badarch, G., Liu, D.Y., 2005. Zircon age and occurrence of the Adaatsag ophiolite and Muron shear zone, central Mongolia: constraints on the evolution of the Mongol–Okhotsk ocean, suture and orogen. Journal of the Geological Society 162, 125–134.
Turcotte, D.L., 1987. Physics of magma segregation processes. In: Mysen, B.O. (Ed.), Magmatic Processes: Physiochemical Principles. The Geochemical Society, Special Publications, No1, pp. 69–74.
Wan, C.B., 2006. Cretaceous palynological flora in Hailar Basin (in Chinese with English abstract). Thesis submitted to Jilin University, Changchun, for the degree of Doctor of Science in Geology.
Wang, Y.L., Hughes, S.S., Tong, C.H., Xiong, S.H., Li, J.C., Zhou, R.S., Li, J.L., 1989. Geochemistry and petrology of Emeishan basalts and subcontinental mantle evolution in southwestern China. Chinese Journal of Geochemistry 8, 37–53.
Wang, P., Ren, Y., Shan, X., Sun, S., Wan, C., Bian, W., 2002. The Cretaceous volcanic succession around the Songliao Basin, NE China: relationship between volcanism and sedimentation. Geological Journal 37, 97–115.
Wang, F., Zhou, X.H., Zhang, L.C., Ying, J.F., Zhang, Y.T., Wu, F.Y., Zhu, R.X., 2006. Late Mesozoic volcanism in the Great Xing'an Range (NE China): timing and implications for the dynamic setting of NE Asia. Earth and Planetary Science Letters 251, 179–198.
Wang, T., Zheng, Y., Zhang, J., Zeng, L., Donskaya, T., Guo, L., Li, J., 2011. Pattern and kinematic polarity of late Mesozoic extension in continental NE Asia: perspectives from metamorphic core complexes. Tectonics. http://dx.doi.org/10.1029/2011TC002896.
Wetherill, G.W., 1956. Discordant uranium–lead ages. Transactions American Geophysical Union 37, 320–326.
Whalen, J., Currie, K., Chappell, B., 1987. A-type granites: geochemical characteristics, discrimination and petrogenesis. Contributions to Mineralogy and Petrology 95, 407–419.
Whalen, J., Jenner, G., Longstaffe, F., Robert, F., Gariepy, C., 1996. Geochemical and isotopic (O, Nd, Pb and Sr) constraints on A-type granite petrogenesis based on the Topsails igneous suite, Newfoundland Appalachians. Journal of Petrology 37, 1463–1489.
Windley, B.F., Alexeiev, D., Xiao, W., Kröner, A., Badarch, G., 2007. Tectonic models for accretion of the Central Asian Orogenic Belt. Journal of the Geological Society 164, 31–47.
Wu, F.Y., Jahn, B.M., Wilde, S., Sun, D.Y., 2000. Phanerozoic crustal growth: U–Pb and Sr–Nd isotopic evidence from the granites in northeastern China. Tectonophysics 328, 89–113.
Wu, F.Y., Lin, J.Q., Wilde, S.A., Zhang, X.O., Yang, J.H., 2005. Nature and significance of the early Cretaceous giant igneous event in eastern China. Earth and Planetary Science Letters 233, 103–119.
Wu, F.Y., Sun, D.Y., Ge, W.C., Zhang, Y.B., Grant, M.L., Wilde, S.A., Jahn, B.M., 2011. Geochronology of the Phanerozoic granitoids in northeastern China. Journal of Asian Earth Sciences 41, 1–30.
Xiao, W.J., Windley, B.F., Hao, J., Zhai, M.G., 2003. Accretion leading to collision and the Permian Solonker suture, Inner Mongolia, China: termination of the Central Asian Orogenic Belt. Tectonics 22. http://dx.doi.org/10.1029/2002TC001484.
Xie, X., Yan, M., Li, L., Shen, H., 1985. Usable values for Chinese standard reference samples of stream sediments, soils, and rocks: GSD 9–12, GSS 1–8 and GSR 1–6. Geostandards Newsletter 9, 277–280.
Xu, W.L., Pei, F.P., Wang, F., Meng, E., Ji, W.Q., Yang, D.B., Wang, W., 2013. Spatial–temporal relationships of Mesozoic volcanic rocks in NE China: constraints on tectonic overprinting and transformations between multiple tectonic regimes. Journal of Asian Earth Sciences. http://dx.doi.org/10.1016/j.jseaes.2013.04.003.
Ying, J.F., Zhou, X.H., Zhang, L.C., Wang, F., Zhang, Y.T., 2010. Geochronological and geochemical investigation of the late Mesozoic volcanic rocks from the northern Great Xing'an Range and their tectonic implications. International Journal of Earth Sciences 99, 357–378.
Zartman, R.E., Doe, B.R., 1981. Plumbotectonics—the model. Tectonophysics 75, 135–162.
Zhang, C.J., Long, Y.W., 1995. Features of Sedimentary Facies and Oil/gas Distribution in Hailar Basin (in Chinese). Petroleum Industry Press, Beijing.
Zhang, Z.C., Mahoney, J.J., Mao, J.W., Wang, F.S., 2006. Geochemistry of picritic and associated basalt flows of the western Emeishan flood basalt province, China. Journal of Petrology 47, 1997–2019.
Zhang, J.H., Ge, W.C., Wu, F.Y., Wilde, S.A., Yang, J.H., Liu, X.M., 2008a. Large-scale early Cretaceous volcanic events in the northern Great Xing'an Range, northeastern China. Lithos 102, 138–157.
Zhang, L.C., Zhou, X.H., Ying, J.F., Wang, F., Guo, F., Wan, B., Chen, Z.G., 2008b. Geochemistry and Sr–Nd–Pb–Hf isotopes of early Cretaceous basalts from the Great Xinggan Range, NE China: implications for their origin and mantle source characteristics. Chemical Geology 256, 12–23.
Zhang, J.H., Gao, S., Ge, W.C., Wu, F.Y., Yang, J.H., Wilde, S.A., Li, M., 2010. Geochronology of the Mesozoic volcanic rocks in the Great Xing'an Range, northeastern China: implications for subduction-induced delamination. Chemical Geology 276, 144–165.
Zhang, F.Q., Chen, H.L., Yu, X., Dong, C.W., Yang, S.F., Pang, Y.M., Batt, G.E., 2011. Early Cretaceous volcanism in the northern Songliao Basin, NE China, and its geodynamic implication. Gondwana Research 19, 163–176.
Zhao, G.L., Yang, G.L., Fu, J.Y., 1989. Mesozoic Volcanic Rocks in the Central-southern Da Hinggan Ling Range (in Chinese). Beijing Press of Science and Technology, Beijing.
Zhao, Z., Chi, X.G., Liu, J.F., Wang, T.F., Hu, Z.C., 2010. Late Paleozoic arc-related magmatism in Yakeshi region, Inner Mongolia: chronological and geochemical evidence (in Chinese with English abstract). Acta Petrologica Sinica 26, 3245–3258.
Zhou, M., Chen, W., Wang, Y., Prevec, S., Liu, P., Howarth, G., 2013. Two stages of immiscible liquid separation in the formation of Panzhihua-type Fe–Ti–V oxide deposits, SW China. Geoscience Frontiers 4, 481–502.
Zindler, A., Staudigel, H., Batiza, R., 1984. Isotope and trace element geochemistry of young Pacific seamounts: implications for the scale of upper mantle heterogeneity. Earth and Planetary Science Letters 70, 175–195.
Zorin, Y.A., 1999. Geodynamics of the western part of the Mongolia–Okhotsk collisional belt, Trans-Baikal region (Russia) and Mongolia. Tectonophysics 306, 33–56.